Title
Environmental durability of silver mirrors with nanostructured protective coatings

Author
Folgner, Kelsey Anne

Publication Date
2016

Peer reviewed|Thesis/dissertation

UNIVERSITY OF CALIFORNIA

Los Angeles

Environmental durability of silver mirrors with nanostructured protective coatings

A thesis submitted in partial satisfaction

of the requirements for the degree Master of Science

in Materials Science and Engineering

by

Kelsey Anne Folgner

2016

ABSTRACT OF THE THESIS

Environmental durability of silver mirrors with nanostructured protective coatings

by

Kelsey Anne Folgner

Master of Science in Materials Science and Engineering

University of California, Los Angeles, 2016

Professor Jenn-Ming Yang, Chair

Highly-reflective silver mirrors are widely used in optical applications. However, silver tarnishes and corrodes in the presence of common atmospheric pollutants, which degrades its reflectivity and optical performance. Various overcoat layers have been developed to protect silver from corrosion, though the mechanisms by which these protective layers improve mirror durability are not fully understood. Accelerated environmental exposure testing was used to investigate the corrosion behavior of protected silver mirrors prepared by plasma beam sputtering. The composition and layered nanostructure of the corrosion features on mirrors with different adhesion layer materials were analyzed. A small amount of nickel in the adhesion layer had a significant impact on adhesion at the silver-dielectric interface, and directly affected the corrosion dynamics. Additionally, lateral migration of silver, not just silver corrosion, was an important factor in the corrosion process. Better adhesion at all layer interfaces is necessary to improve mirror durability.

The thesis of Kelsey Anne Folgner is approved.

Ya-Hong Xie

Yang Yang

Jenn-Ming Yang, Committee Chair

University of California, Los Angeles

2016

Table of Contents

List of Figures

List of Tables

Acknowledgements

I would like to acknowledge the contributions of those who made this work possible, and to express my gratitude for their continual support.

From the Aerospace Corporation, I would like to acknowledge Dr. James Barrie, for his thin film expertise and guidance, and Dr. Chung-Tse Chu, for his support in conducting the testing and for many useful discussions. I would also like to thank: Dr. Peter Fuqua, for many helpful conversations; Mr. Christopher Panetta, Mrs. Diana Alaan, and Mr. Paul Adams, for their assistance in characterizing the coatings; Dr. Hyun Kim, for his assistance with XPS; and Dr. Zachary Lingley, Mr. Miles Brodie, and Mr. Scott Sitzman, for their help with the TEM and FIB. I would further like to acknowledge the support and encouragement of my management, Dr. Sherrie Zacharius, Dr. James Nokes, and Dr. Shant Kenderian, as well as the support of the Aerospace Fellowship Program. Finally, I would like to sincerely thank Dr. Rafael Zaldivar, for his continuous support and advice, and for his boundless motivation and enthusiasm.

From UCLA, I would like to acknowledge my advisor, Professor Jenn-Ming Yang, for his guidance and support. I would also like to thank Professor Ya-Hong Xie and Professor Yang Yang for their service on my thesis committee.

This work was funded and supported by The Aerospace Corporation's Independent Research and Development program. A version of this thesis is in preparation for publication.

1. Introduction

High-reflectivity silver mirrors are widely used in optical applications [1 – 6]. Silver possesses the highest reflectivity, lowest emissivity, and lowest polarization splitting of all metals, making it the material of choice for the most demanding visible and infrared applications [2, 3, 5, 7]. However, silver is also widely known to tarnish and corrode in the presence of common atmospheric pollutants, which degrades its reflectivity and optical performance [3, 7 – 11]. Various schemes have been developed to protect thin film silver mirrors from tarnish and corrosion during long-term environmental exposure [1, 4, 5, 9, 12 – 14]. While these protection layers are necessary to improve mirror durability and increase the lifetime of the coating, they are not always sufficient to prevent eventual degradation [1, 4, 11]. In addition, they often reduce the excellent initial optical performance of silver. Moreover, the mechanisms by which these various protection layers improve mirror durability are not fully understood.

This thesis will investigate the corrosion behavior of protected silver mirrors in an attempt to elucidate the nature of the protection mechanisms. A relatively new sputtering technique will be employed to deposit high-quality silver mirrors with various protection layers. Accelerated environmental exposure testing will then be used to simulate atmospheric corrosion of the silver coatings. Various analytical techniques will be utilized to investigate the optical properties of the silver mirrors, their nanostructure, and the resulting corrosion features. The goal is to improve our understanding of corrosion resistance to enable the deposition of more durable mirrors.

2. Background and theory

2.1 Silver

While silver has long been prized as a precious metal, its extraordinary properties also make it an important technological material. Silver is a soft, lustrous metal with good ductility and malleability. It has the highest electrical and thermal conductivity of any metal [7, 8]. Optically, silver has the highest broad-band reflectivity with the corresponding lowest emissivity, as well as the lowest polarization splitting among metals [2, 3, 5, 7]. The theoretical reflectivity of silver is 97.9% at 500 nm and improves at longer wavelengths to better than 99% [13]. However, the reflectivity of silver does decrease in the ultra-violet (UV) spectrum, dropping to near zero at approximately 320 nm due to surface plasmon resonance [3, 12].

Even so, its excellent optical properties make silver well-suited for use in high-reflectivity mirror applications when compared to other highly-reflecting metals, such as gold and aluminum. While gold has comparably high infrared reflectivity and corresponding low infrared emissivity, it has significant absorption in the visible spectrum, as shown in Figure 1 [4, 13]. Aluminum maintains moderate reflectivity across the UV, visible, and infrared (IR) spectrums, and is the material of choice for UV applications. However, its visible reflectivity is significantly lower than that of silver and its infrared emissivity is substantially higher [4, 13]. Furthermore, aluminum exhibits interband absorption at 800 nm, which leads to a reflectivity 10% lower than that of silver.

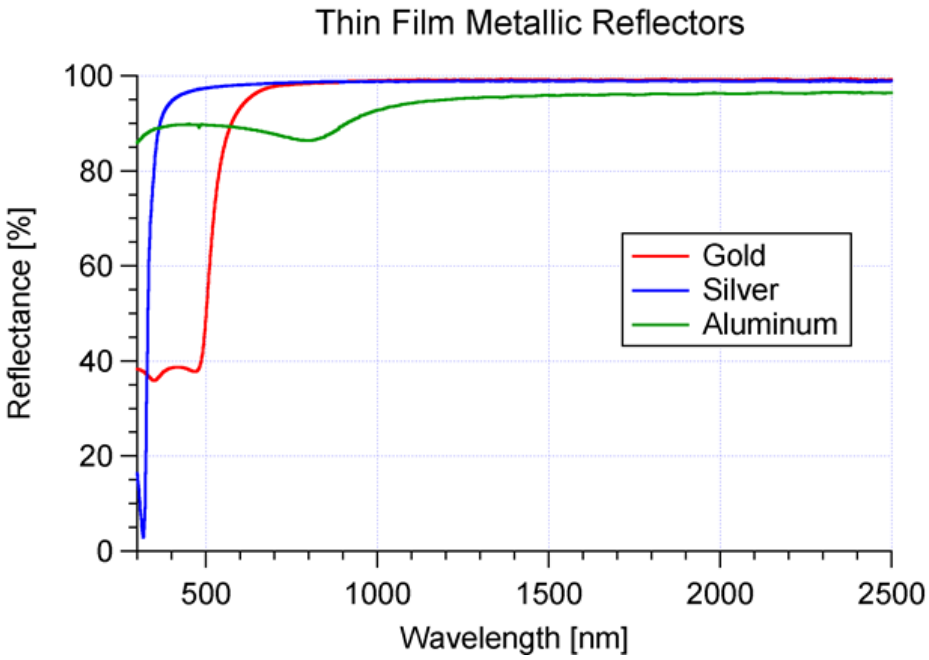

Figure 1. Reflectance spectra of common mirror materials.

2.1.1 Silver corrosion

While the optical properties of silver surpass those of aluminum and gold, silver is known to tarnish and corrode much more readily when exposed to common atmospheric pollutants [3, 4, 7 – 11, 13]. Gold naturally resists atmospheric corrosion well, while aluminum develops a protective oxide coating that prevents corrosion with minimal impact to its optical performance. Silver has no such protective coating or natural resistance to corrosion. The tarnish and corrosion that develops on silver degrades its reflectance and increases its scatter, vastly reducing its optical performance [7, 9, 10].

Although it is a noble metal, silver reacts readily with sulfur and halogen compounds in the environment [7, 8, 15]. Silver does not easily oxidize, even though its oxide is stable at room temperature [7]. Rather, silver sulfide (Ag_2S), a highly absorbing compound, is the most common tarnish or corrosion observed on silver surfaces [7, 14]. The brown or black patina of Ag_2S

develops on silver upon exposure to trace amounts of pollutants in common air. This patina does not cause significant metal loss, but degrades silver's high reflectivity and must be removed by polishing [7]. While Ag_2S is the most common corrosion product, silver chloride (AgCl), silver oxide (Ag_2O), and silver sulfate (Ag_2SO_4) have also been observed [3, 7, 8, 14, 15].

Silver is known to corrode in various environments; the presence of hydrogen sulfide (H_2S), ozone (O_3), hydrogen chloride (HCl), hydrogen peroxide (H_2O_2), and sulfur dioxide (SO_2) have been observed to initiate corrosive reactions with silver [3, 7, 8, 14, 15]. While H_2S is the most common tarnishing agent, there is believed to be a synergistic effect from multiple reactants that increases silver corrosion [6, 8]. In addition, the presence of oxygen and water vapor significantly accelerates silver corrosion reactions [6 – 8]. Eliminating moisture through low relative humidity is believed to be more effective in preventing silver corrosion than trying to reduce the small amount of trace pollutants in the environment [6, 8].

2.2 Thin film silver mirrors

Front surface silver mirrors are configured to maximize the exceptional optical properties of silver by utilizing the highly-reflective silver surface directly [13]. The mirrors are constructed by depositing a thin layer of silver on a backing substrate, often glass. Light incident on the mirror strikes the silver without first travelling through the glass, which significantly improves mirror performance and reduces ghosting effects. However, front surface silver mirrors leave the reflective surface of the bare silver exposed to the potentially corrosive species in the environment [7]. In addition, silver suffers from poor adhesion to common substrate materials [6]. Research on these durability issues extends back into the 1960s [4, 7, 10, 13, 14, 16].

2.2.1 Protection layers

Protective layers on top of the thin silver layer can be used to protect the bare silver from corrosion [4, 13, 14, 16]. These protective overcoat layers should be transparent, with low scatter, to minimize their impact on the silver reflectance [14]. In addition, they should be deposited with a minimum of defects and pinholes to prevent corrosive species from reaching the silver. Finally, materials with low diffusion rates for silver are preferred because silver is known to be highly mobile.

Various protective overcoat materials have been utilized alone and in combination. These include metal oxides, nitrides, and fluorides such as silica (SiO_2), silicon monoxide (SiO), alumina (Al_2O_3), hafnia (HfO_2), tantala (Ta_2O_5), silicon nitride (Si_3N_4), magnesium fluoride (MgF_2), and yttrium fluoride (YF_3) [1, 4, 5, 9, 12 – 14, 16]. These transparent dielectric materials can be used as single layers to provide improved corrosion resistance to the silver. They can also be used as multilayer stacks to further improve durability. When used as alternating layers of materials with high and low refractive indices, there can be the added benefit of increasing the silver reflectance by means of interference enhancement [5, 14]. However, these extra layers do have some penalty in emittance and reflectance at wavelengths where their interference effect is destructive [14]. Ultimately, the optical properties of the protection layers must be optimized for the specific application.

2.2.2 Adhesion layers

While the protective layers alone afford protection to the silver, good adhesion of the dielectric layers to the silver layer is extremely important in achieving improved mirror durability [1, 4, 5, 9, 11 – 14, 17]. One way to improve the adhesion of the dielectric to the silver is the

addition of a thin interlayer that bonds well to both [9, 11, 12]. Typical "adhesion layers" include titanium, chromium, and nichrome (NiCr, usually nickel-chromium 80/20 wt. %), as well as metal oxides such as alumina, and metal nitrides such as chromium nitride (CrN_x) and nichrome nitride ($NiCrN_x$) [1, 4, 5, 9, 11 – 14, 16, 17]. The stoichiometry of the nitride adhesion layers is not usually known due to the nature of the reactive deposition process. In general, the adhesion layers are usually very thin, on the order of 10Å or less, to minimize their deleterious effects on the silver reflectance. When incorporated into protected silver mirrors, however, these adhesion layers can dramatically improve corrosion resistance [1, 3, 9, 11, 12]. Use of these adhesion layers is, then, a balance between optical performance and durability.

Relatedly, a second "adhesion layer" is also often used between the substrate and the silver layer to improve the adhesion of the silver to the substrate [9, 12]. This layer is generally, though not always, thicker than the adhesion layer discussed above. It is usually made with the same materials, though copper has also been used effectively [4]. This lower adhesion layer also helps protect the silver from corrosive species.

2.2.3 Durable silver mirrors

Various protection and adhesion layer schemes have been developed to improve mirror durability. Wolfe et al. developed one such scheme based on two thin adhesion layers of $NiCrN_x$, one on each side of the silver layer, followed by a protective overcoat of SiN_x on top of the tri-layer [12]. They found that a $NiCrN_x$ adhesion layer provided the optimal balance between durability and optical performance when compared to the other materials tested [12]. While the $NiCrN_x$ adhesion layer substantially improves mirror durability, it reduces the reflectance of the mirror, particularly in the blue region of the visible spectrum. To balance these two competing

effects, the researchers found that the $NiCrN_x$ layer could be as thin as 8Å and still afford substantial protection against corrosion without significantly limiting optical performance [12]. This coating scheme has been used in several telescope applications with reasonable success [1, 5, 16].

Wolfe et al. reported that $NiCrN_x$ is an effective adhesion layer because it is believed to deposit as an admixture of Ni and CrN_x [12]. As neither nickel nor silver is expected to form a nitride under these deposition conditions, a metal-to-metal bond is believed to form between the two. CrN_x, on the other hand, is believed to form a chemical bond with the SiN_x overcoat. Together, this improves adhesion at the silver-dielectric interface. Additionally, Wolfe et al. found that $NiCrN_x$ is not an effective barrier to corrosion on its own; the SiN_x overcoat is also required [12]. Their data suggested this was because the $NiCrN_x$ was not continuous, but rather, deposited as islands.

Fuqua and Barrie, and later Chu et al., have reported that the thin $NiCrN_x$ adhesion layer provides nucleation sites for the growth of a dense and, therefore, effective SiN_x protection layer [11, 18]. Their work with electrochemical impedance spectroscopy (EIS) indicates that the $NiCrN_x$ affords protection to the silver by reducing porosity in the SiN_x protection layer. By decreasing the permeability of the protection layer, corrosive species cannot penetrate through to react with the silver. More recent EIS work by Ben Amor et al. further supports this mechanism [17]. All of these researchers speculate that a delaminated zone between the dielectric and silver layers develops when corrosive species are allowed to penetrate through a porous SiN_x layer, leading to further corrosion [11, 17, 18]. The $NiCrN_x$ "adhesion layer" prevents this delamination.

2.2.4 Current work

In addition to the work described above, silver mirror durability continues to be an active area of research. In our laboratory, Chu et al. have investigated additional accelerated environmental exposure tests to assess mirror durability [19]. Relatedly, Barrie et al. have investigated the effects of film stress on corrosion behavior [9]. Elsewhere, Philips et al. have explored numerous adhesion layer materials, as well as various nitride and fluoride protection layers, in an attempt to improve overall durability [20]. They have also compared several deposition processes to improve layer integrity and limit porosity [21]. In addition, Sheikh continues to report on the development of UV-enhanced protected silver mirrors [16].

Schwinde et al. have further investigated one mechanism of corrosion in protected silver mirrors [22]. They report a particle-induced damage mechanism whereby hygroscopic airborne particles are adsorbed on the mirror surface. These particles attract water from the environment, eventually forming droplets that contain dissolved elements, notably sulfur and chlorine. They suggest that the droplet solution weakens the protective layer, permeates the coating, and leads to silver corrosion. Their work supports the necessity of dense, non-porous protection layers and the requirement for clean, dry environments to prevent silver corrosion. It further demonstrates the ongoing need for more durable silver mirrors.

While the protection and adhesion layers are necessary to improve corrosion resistance, they are not sufficient to afford absolute protection [1, 5, 9, 11, 19 – 22]. The search for more durable silver mirrors continues. Better adhesion layer materials that do not significantly reduce the reflectance of silver are required. Developing these new materials demands a better understanding of the mechanisms by which $NiCrN_x$ and other adhesion layer materials afford corrosion protection to the silver mirrors.

2.3 Silver mirror deposition

While thin films can be prepared by a number of physical vapor deposition techniques, sputtering is one process of choice for high-quality protected silver mirrors [23]. For example, magnetron sputtering has been used extensively to deposit durable silver mirrors [1, 11, 12, 18, 19, 22].

The sputter deposition process begins with the bombardment of a solid target material by energetic ions generated by a plasma [23, 24]. The ions have sufficient energy to eject, or sputter, atoms from the target surface through momentum transfer. The sputtered atoms condense on the substrate surface, producing the thin film. Typically, an inert sputtering gas such as argon is used to enable and sustain the plasma. The creation and maintenance of a high density plasma during the sputtering process produces higher-quality coatings [25]. In addition, magnets can be used to confine and control the plasma near the target, such as in magnetron sputtering. This increases the ionization efficiency and yields higher deposition rates [23].

A relatively new sputtering technique, known as plasma beam sputtering, utilizes a high-density plasma source to produce high-quality thin films [9, 25]. The high-density, inductively-coupled, radio frequency (RF) plasma is generated external to the deposition chamber. The plasma is then magnetically steered and electrically accelerated towards the target for sputtering. Exciting the plasma remotely from the sputtering environment enables the independent control of process variables that cannot be separated in conventional sputtering processes. Ion density and ion energy are decoupled in plasma beam sputtering, allowing the structure and properties of the film to be tailored in novel ways [25].

2.4 Accelerated environmental exposure

Accelerated environmental exposure tests are designed to evaluate the long-term behavior of materials in a shortened time frame. Various accelerated tests have been used to evaluate protected silver mirrors, including humidity exposure, acid-vapor exposure, salt fog exposure, and, more recently, mixed flowing gas (MFG) exposure [3 – 5, 9, 11, 12, 16, 18, 22, 26, 27]. While salt fog and humidity exposures have been de facto standards for assessing mirror durability, MFG exposure has recently been considered a more realistic assessment of long term behavior [19, 28, 29].

MFG exposure testing was developed in the 1980's as an accelerated environmental test to evaluate the reliability of electrical components [27, 28, 30]. MFG exposure conditions were designed to simulate corrosion resulting from common atmospheric pollutants. Chu et al. have recently applied these tests to both silver and gold mirrors to assess durability; their work indicates good agreement between the corrosion behavior observed during MFG testing and that observed during long-term environmental exposure [19, 28, 29]. For testing, the protected silver mirrors are exposed to specific concentrations of three known air pollutants, hydrogen sulfide, chlorine (Cl_2), and nitrogen dioxide (NO_2), along with moisture at a constant relative humidity. The testing environment simulates an indoor environment such as a business office or laboratory that does not have effective or continuous environmental control [30].

3. Experimental

3.1 Plasma beam sputtering

Thin film silver mirrors with various adhesion and protection layers were deposited via plasma beam sputtering in a custom deposition chamber, shown in Figure 2. The custom 0.9 m deposition chamber contains the plasma source, an electrically-biased, water-cooled target holder for four 15.24 cm diameter targets, and a continuously rotating sample holder for 5.08 cm samples. The target materials used in this study are specified in Table 1. The deposition process is fully automated, including the RF source power, the DC target bias, and the steering electromagnet current.

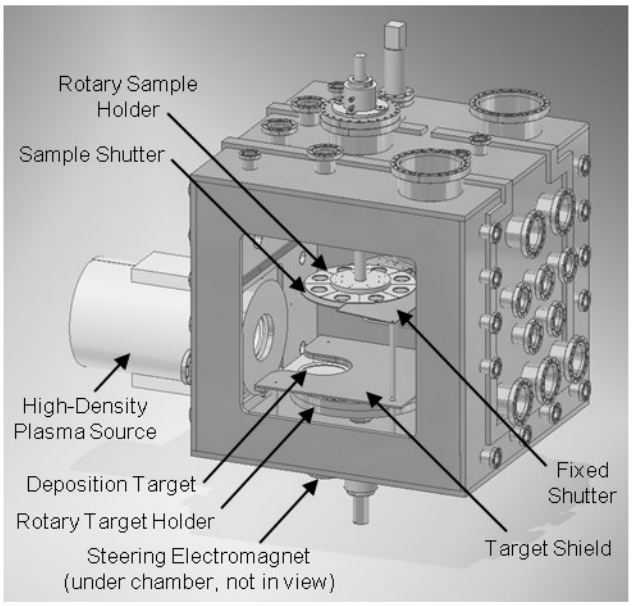

Figure 2. Custom plasma beam sputtering system.

Table 1. Target Material Specifications

Target Name	Target Material	Purity (%)
Chromium	Cr	99.95
Nichrome	NiCr 80/20 wt. %	99.95
Silver	Ag	99.99
Silicon	Si (P-type)	99.999

For each deposition, prime-quality polished silicon wafers were loaded into the sample holder and the chamber was pumped to a base pressure of approximately 3×10^{-7} Torr. The chamber was then backfilled with argon gas at 40 SCCM (cubic centimeters per minute at standard temperature and pressure) to a pressure of 2.0 mTorr, which was controlled with a vane throttling valve and a CTI-Cryogenics CTI-8 cryopump. The mirror layers were then deposited according to the recipe shown in Table 2. During reactive deposition of the nitride layers, additional N_2 gas flowed at a rate of 14.6 SCCM for CrN_x and 12.6 SCCM for $NiCrN_x$ and SiN_x.

Table 2. Deposition Conditions for Silver Mirrors

Layer	Material	Thickness (Å)	Rate (Å/min)	Target	RF Power (W)	Target Bias (W)
1	NiCr	200	78	Nichrome	1000	1000
2	Ag	1200	228	Silver	1000	1000
3	Option 1: $NiCrN_x$	0 to 10	84	Nichrome	1000	1000
	Option 2: CrN_x		42	Chromium	1000	1000
4	SiN_x	100	24	Silicon	1300	1000

The four layer mirror design consists of a thin NiCr layer for adhesion of the silver to the silicon substrate, a thick silver reflective layer, a very thin $NiCrN_x$ or CrN_x interlayer for adhesion of the protective dielectric layer to the silver, and a single dielectric overcoat layer of SiN_x for corrosion protection of the silver. Additionally, mirrors without any adhesion layer (Layer 3) or protection layer (Layer 4) were deposited for this study. The entire coating stack is 150 nm thick.

Layer thickness was controlled by quartz crystal monitors. QCM calibration factors were determined by ellipsometry, using a J.A. Woollam Variable Angle Spectroscopic Ellipsometer (VASE), or profilometry, using a Keyence VK-X200 3D laser scanning confocal microscope. For the very thin layers, the calibration factors were determined for thicker films and do not account for issues, such as the time of shutter actuation, that are no longer negligible during very short depositions. Ellipsometry was also used to measure the index of refraction of the dielectric layers.

3.2 Accelerated environmental exposure testing

Durability and corrosion resistance of the mirrors were evaluated with two different accelerated environmental exposure tests. Salt fog exposure was conducted in a BEMCO P700XL salt-spray chamber maintained at 95°F with a 5% NaCl solution sprayed at a rate of 1.0 – 2.0 ml/hr, as specified by ASTM B117 [26]. The samples were tested for durations between 2 and 16 hours. Under these conditions, most silver mirrors exhibit significant corrosion and degradation [9].

Mixed flowing gas exposure was conducted in a custom 3.75 ft^3 acrylic test chamber. Three known air pollutants, H_2S, Cl_2, and NO_2, were utilized at specific concentrations by diluting with purified air produced by a Parker Balston 76-98-N100 zero air generator. Specific test conditions are given in Table 3 as described by the Battelle Laboratory MFG Test Methods Class II environment for testing electronic components [30]. The Class II environment simulates an indoor environment such as a business office or laboratory that does not have effective or continuous environmental control [27, 30]. A bubbler was used to introduce moisture into the gas flow and control the relative humidity in the test chamber. The gases were supplied in certified gas cylinders. H_2S (10 ppm in N_2) and NO_2 (100 ppm in N_2) were supplied by Scott-Marrin, Inc. and Cl_2 (20 ppm in N_2) was supplied by Matheson Tri-Gas, Inc. The H_2S and NO_2 concentrations

were monitored continuously with Teledyne-API gas analyzers, models M101E and M200, respectively. Cl_2 was monitored with a Particle Measuring Systems AirSentry II Chlorine Analyzer. The mirror samples were tested for a total of 10 days (242 hr), in increments of two to three days at a time. Chu et al. has shown that RF magnetron sputtered bare silver mirrors, as well as those without adhesion layers, significantly degrade under these conditions [19].

Table 3. Test Conditions for Mixed Flowing Gas Exposure

Method	H_2S (ppb)	Cl_2 (ppb)	NO_2 (ppb)	Temperature (°C)	Relative Humidity (%)
Class II	10	10	200	30	70

3.3 Mirror characterization

Prior to environmental exposure testing, the mirrors were pre-characterized to determine baseline optical properties and film morphology. During environmental testing, the exposures were periodically stopped to characterize on-going changes in properties and morphology. Finally, the mirrors were post-characterized after environmental testing with additional analytical techniques.

3.3.1 Optical properties

Reflectance was measured at the mirror center from 200 to 2500 nm with a Perkin-Elmer Lambda 950 spectrometer with an absolute reflectance accessory (URA). Scatter was measured with a Schmitt Measurement Systems (SMS) μ-scan scatterometer at 670 nm. This instrument measures the bidirectional reflectance distribution function (BRDF) at two angles to calculate an equivalent surface roughness from the measured scatter.

3.3.2 Film morphology

Optical microscopy was utilized to image the mirror surfaces to observe changes in film morphology. A Keyence VHX-600 digital microscope was used under oblique (dark field) lighting conditions to highlight degradation on the entire mirror surface. A Nikon Eclipse LV100 optical microscope was used for higher magnification imaging of specific surface features under bright field, dark field, and differential interference contrast (DIC) modes. The as-deposited mirrors were pre-characterized to document coating defects that could potentially affect mirror durability.

3.3.3 Film microstructure

Following environmental testing, detailed surface observations and elemental analyses were performed using a JEOL JSM-7600F scanning electron microscope (SEM) equipped with an energy dispersive X-ray microanalyzer (EDS). Micrographs were obtained in secondary electron and backscatter electron modes under an accelerating voltage of either 15 kV or 2 kV. EDS spectra were obtained at 15 kV.

In addition, several mirror coatings were cross-sectioned for imaging of the layers and their structure in a transmission electron microscope (TEM). Images were collected with a JEOL 3100F TEM operated at 300kV in scanning transmission mode (STEM). Two imaging modes were used. Z-contrast (density) images were collected in high angle annular dark field mode (HAADF) and diffraction contrast images were collected in annular dark field mode (ADF). Energy dispersive X-ray spectroscopy (EDS) data were collected with a 30 mm^2 Oxford silicon-lithium detector. TEM specimens were prepared from the mirrors by the focused ion beam (FIB) lift-out method on an FEI Strata 400 with an in-situ sample manipulation probe and in-situ platinum deposition [31].

Final thinning was performed at 2 kV to minimize the thickness of the amorphous layer. Care was taken to minimize air exposure of the prepared TEM specimens to prevent exposed silver from reacting with the environment.

3.3.4 Elemental analyses

X-ray photoelectron spectroscopy (XPS) was utilized to measure the elemental composition of the as-deposited mirrors using a Physical Electronics, Inc. VersaProbe II Scanning XPS Microprobe. To investigate the layers of the mirror coatings, XPS depth profiles were obtained by combining a sequence of ion sputter etch cycles interleaved with XPS elemental compositional analyses. The mirror surface was etched by rastering a 1 keV Ar ion beam over a 2 mm × 2 mm area. The etch rate was 0.55 nm/min. After each sputter cycle, elemental compositional analysis was performed on the center of the sputtered area. A 200 μm diameter X-ray beam was used to generate photoelectrons from the surface, which were then collected and analyzed with a hemispherical analyzer. The generated photoelectron spectrum consists of the number of photoelectrons collected at specific binding energies. The measured photoelectron binding energy represents the energy to remove electrons from atoms and is used for elemental identification. Using the relative photoelectron count at each binding energy as well as tabulated photoelectron yields, the composition of the surface can be calculated in terms of relative atomic percent. For this study, the analyzer pass energy was 46.95 eV and the XPS analysis chamber was ion pumped to a base pressure of 1×10^{-10} Torr.

4. Plasma beam sputtered silver mirrors

4.1 Optical properties

Silver mirrors deposited by plasma beam sputtering exhibit excellent broad-band reflectance across the visible and infrared spectrum [9]. As shown in Figure 3, a thin film, plasma beam sputtered bare silver mirror has greater than 97% reflectance above 500 nm. The reflectance drops significantly below 400 nm due to surface plasmon resonance [3]. The addition of various adhesion and protection layers on top of the silver is known to increase mirror durability, but can significantly reduce reflectance [3, 4, 9, 12, 13, 16, 18]. Figure 3 shows the effect of adding a very thin layer of $NiCrN_x$ on top of the silver layer. Figure 4 shows the effect of adding both a thin $NiCrN_x$ adhesion layer as well as a dielectric protection layer of 100Å of SiN_x. The adhesion and protection layers dramatically decrease reflectance, even for just 3Å of $NiCrN_x$.

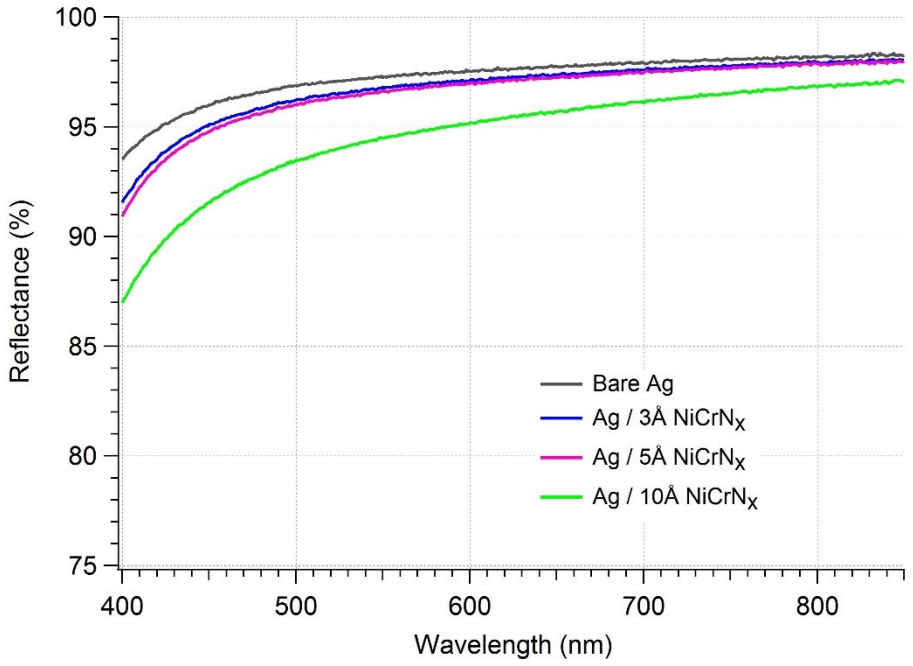

Figure 3. Reflectance spectra of silver mirrors prepared by plasma beam sputtering. Reduced reflectance is evident due to very thin layers of $NiCrN_x$.

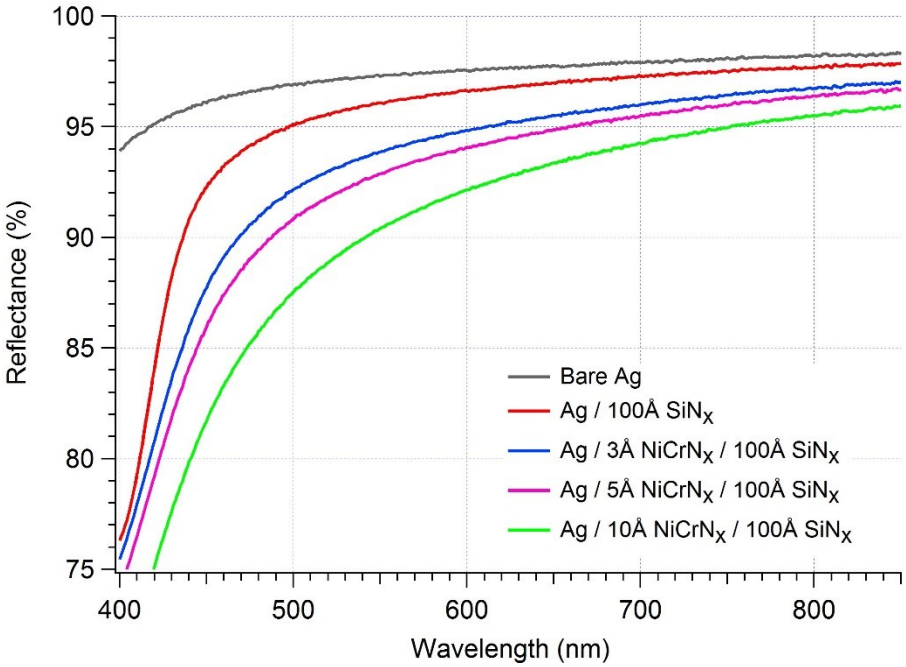

Figure 4. Reflectance spectra of silver mirrors prepared by plasma beam sputtering. Reduced reflectance is evident due to a 100Å SiN_x dielectric protection layer as well as $NiCrN_x$ adhesion layers of various thicknesses.

In addition to $NiCrN_x$, CrN_x was used as an adhesion layer in this study. The reflectance for a protected silver mirror with a 5Å CrN_x adhesion layer is shown in Figure 5. A mirror with a 5Å CrN_x adhesion layer is expected to have a higher reflectance than an identical mirror with a 5Å $NiCrN_x$ adhesion layer due to the absence of nickel. The nickel is metallic and, therefore, more absorptive than the CrN_x, which is only slightly absorbing. The small difference in reflectance for the two adhesion layer mirrors in Figure 5 suggests that either the CrN_x layer is thicker, and therefore the CrN_x adhesion layer mirror is less reflective, than expected; or, conversely, that the $NiCrN_x$ layer is thinner, and therefore the $NiCrN_x$ adhesion layer mirror is more reflective, than expected. The focus of this study was on the role of the adhesion layer in preventing mirror degradation, not on specific adhesion layer thicknesses. As such, the comparable reflectance of the CrN_x and $NiCrN_x$ mirrors provides a similar starting point for assessing differences in degradation and corrosion phenomena.

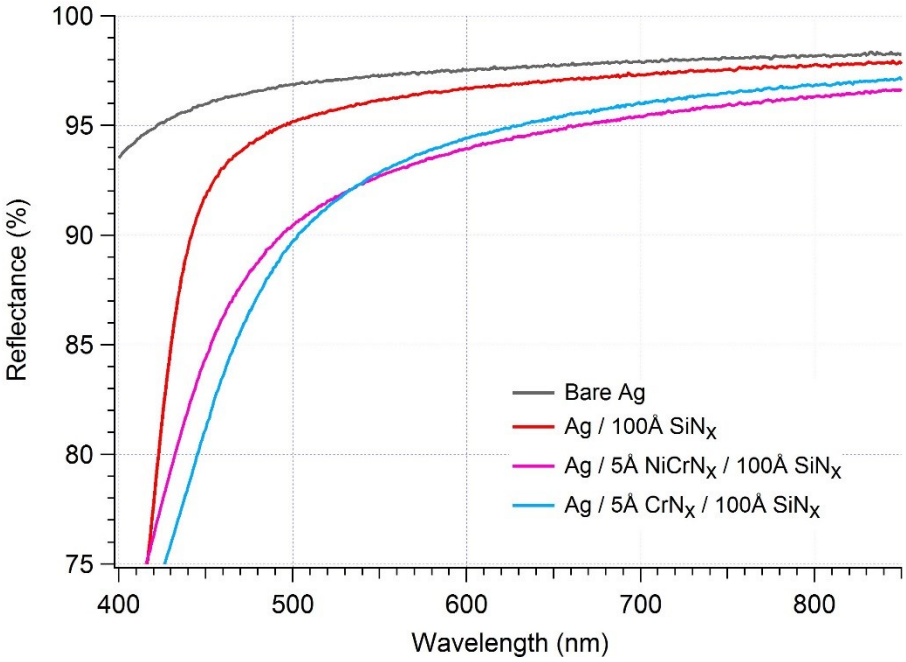

Figure 5. Reflectance spectra of silver mirrors prepared by plasma beam sputtering comparing adhesion layers of $NiCrN_x$ or CrN_x.

Scatter from these plasma beam sputtered silver mirrors is very low, with measured BRDF levels usually below 5×10^{-5}/sr. The addition of the adhesion and protection layers increases the measured scatter slightly compared to bare silver mirrors, which measured at 2.5×10^{-5}/sr.

Compared to RF magnetron sputtered silver mirrors previously produced in our laboratory, the plasma beam sputtered mirrors in this study exhibit slightly reduced optical performance [11, 18]. The reflectance is slightly lower, and the scatter is slightly higher. This is believed to be at least partially due to arcing that occurs during DC bias deposition of the nitrides, which makes those layers more absorptive. In addition, the silver layer is rougher than expected. These differences are mentioned for completeness, but are not expected to affect the comparative results of this study.

4.2 Layer nanostructure

The nanoscale layered structure of a plasma beam sputtered silver mirror with a nominal 10Å $NiCrN_x$ adhesion layer is shown in Figure 6. The polished silicon substrate is evenly coated with a uniform layer of NiCr, nominally 200Å thick. The silver layer follows and develops substantial roughness as the layer grows. This is not unexpected, as coarsening during layer growth is well known [32, 33]. The subsequent thin $NiCrN_x$ adhesion layer and the 100Å SiN_x protection layer are deposited conformally on the silver. The SiN_x is visible as a dark gray layer following the undulations of the silver. The highly topographic Ag-$NiCrN_x$-SiN_x interface prevents direct imaging and thickness measurements of the thin $NiCrN_x$ adhesion layer. STEM imaging includes information through the entire thickness of the TEM specimen. With the scale of the undulations on the order of the TEM specimen thickness, through thickness effects are apparent in the image due to the overlapping undulations.

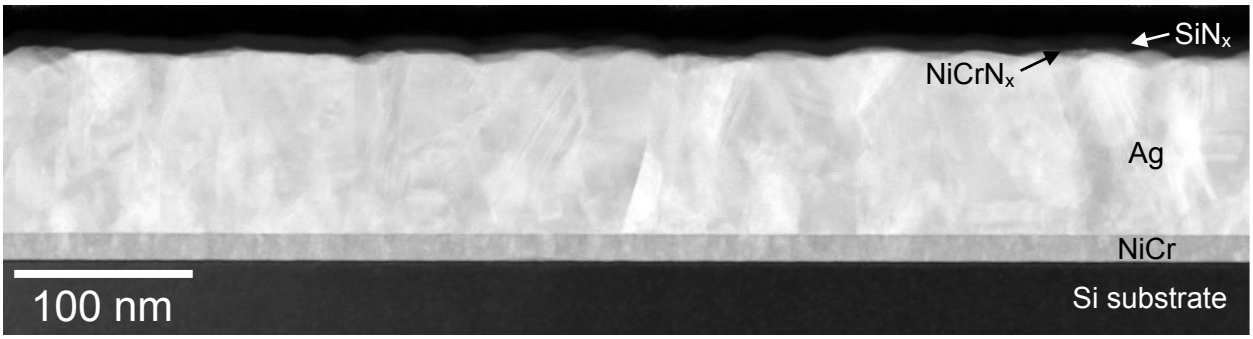

Figure 6. ADF-STEM image of a cross-section of 100Å SiN_x over 10Å $NiCrN_x$ over Ag.

Close inspection of Figure 6 reveals that the layers are thinner than expected. Based on calibration of deposition rate and layer thickness, the silver layer was expected to be 1200Å. It appears to be slightly over 1000Å in the ADF-STEM image; exact measurement is difficult due to the roughness at the top of the Ag layer. The SiN_x and NiCr layers are similarly thinner than

expected. These thickness differences are mentioned for completeness, but should not impact the testing and analysis performed in this study.

To further characterize the nano-layered structure, EDS maps of the top portion of the mirror coating are shown in Figure 7. The line behind the images marks the nominal position of the 10Å $NiCrN_x$ adhesion layer. The nickel and chromium signals clearly indicate the $NiCrN_x$ layer is present and follows the topography of the silver layer. The data suggest that the $NiCrN_x$ layer is continuous; there is no reason to believe it has deposited as islands, as Wolfe et al. have indicated [12]. However, limitations in EDS spatial resolution and low signal-to-noise make it difficult to determine the exact morphology of the $NiCrN_x$ layer. Even so, the sharp distinction between the silicon and silver signals seems to indicate the layered structure is preserved at this interface.

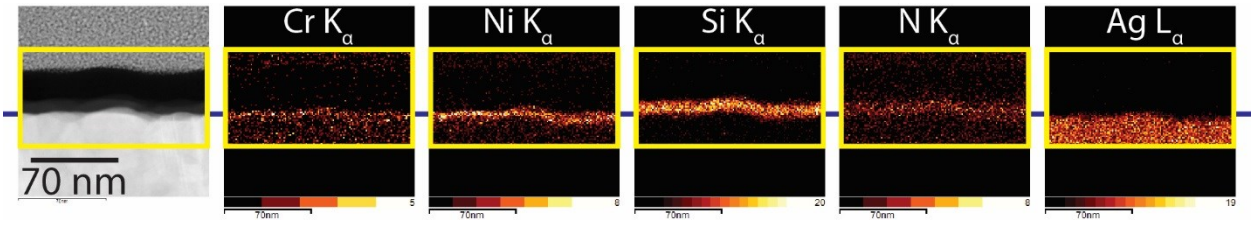

Figure 7. EDS maps of a cross-section of 100Å SiN_x over 10Å $NiCrN_x$ over Ag. The $NiCrN_x$ layer is clearly present and appears continuous, following the undulations of the silver layer.

4.3 Layer composition

XPS depth profiles of protected silver mirrors with 5Å $NiCrN_x$ and 5Å CrN_x adhesion layers are shown in Figure 8 and Figure 9, respectively. The vertical lines indicate the time corresponding to 100Å of sputtered material to show the approximate location of the adhesion layer. Due to the nature of the XPS sputter etch cycles, the layer interfaces do not appear abrupt. Even so, the asymmetry of the nickel signal in the depth profile of the $NiCrN_x$ adhesion layer

mirror suggests that the nickel penetrates further into the silver than its 5Å thickness would imply. This is further supported by the nickel signal extending into the silver further than the nitrogen signal. This suggests that the CrN_x and the Ni behave differently in the adhesion layer. A comparable penetration effect is not evident for the chromium signal in the CrN_x adhesion layer mirror. An understanding of the exact nature of the nickel-silver interaction is not available from this data. However, it is possible that nickel has diffused into the silver to some degree. This could serve to promote better adhesion between the silver layer and the protective SiN_x overcoat layer, helping to prevent silver corrosion and coating degradation.

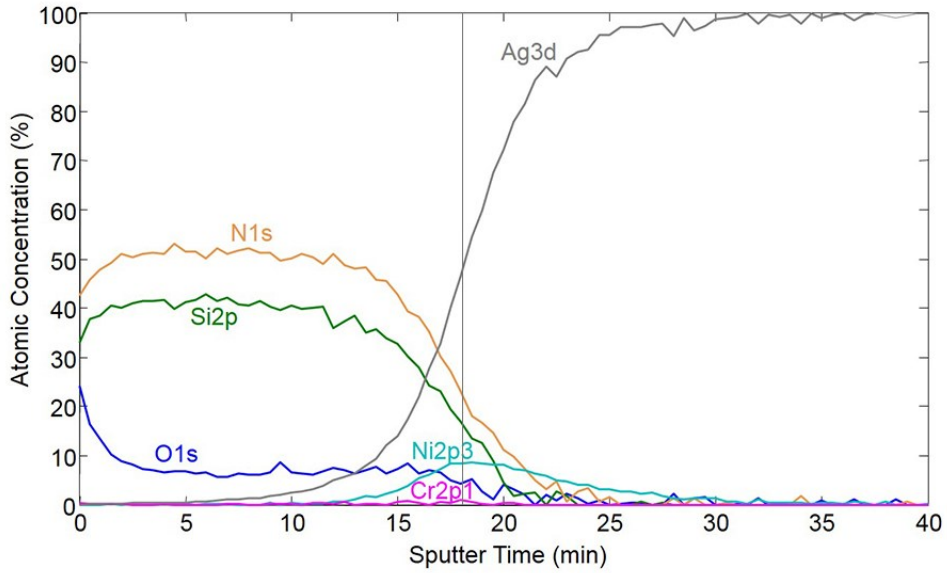

Figure 8. XPS depth profile of 100Å SiN_x over 5Å $NiCrN_x$ over Ag.

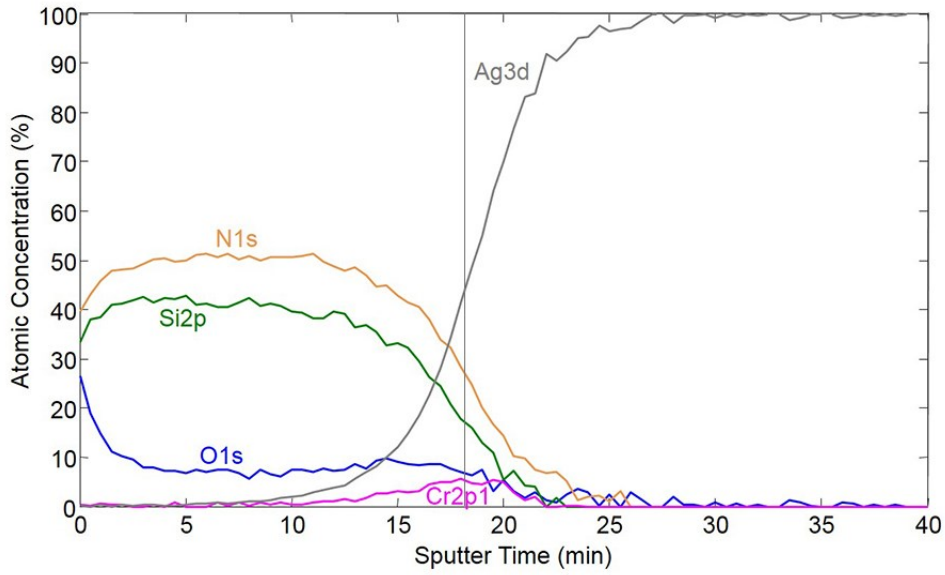

Figure 9. XPS depth profile of 100Å SiN_x over 5Å CrN_x over Ag.

5. Durability of plasma beam sputtered silver mirrors

The durability and corrosion resistance of plasma beam sputtered silver mirrors were investigated through two accelerated environmental exposure tests. These tests are intended to simulate the mechanisms of degradation due to long-term environmental exposure.

5.1 Salt fog exposure

Bare silver mirrors are known to degrade significantly during salt fog exposure [11, 18]. The reflectance spectra of a bare silver mirror tested for 4 hours in salt fog are shown in Figure 10. The reflectance dropped nearly 15% at 500 nm after this short exposure.

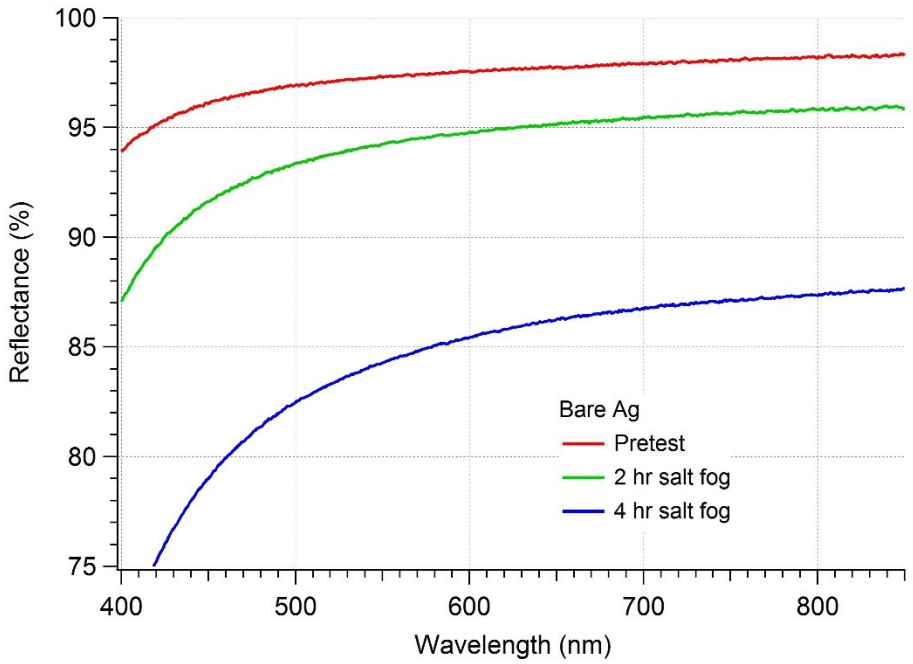

Figure 10. Reflectance spectra of a bare silver mirror before and after salt fog exposure.

In addition, the measured scatter increased nearly three orders of magnitude, from 2.6×10^{-5}/sr pretest to 2.3×10^{-2}/sr after 4 hours of salt fog exposure. The increased scatter of

the severely degraded bare silver is evident in the dark field images shown in Figure 11. The reduction in reflectance is largely due to the increased scatter.

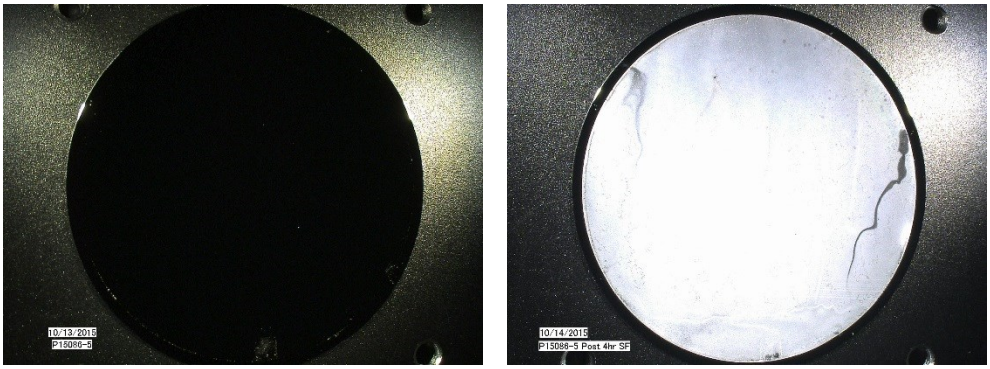

(a) (b)

Figure 11. Dark field images of a bare silver mirror (a) before and (b) after 4 hr salt fog exposure.

The addition of a thin dielectric protection layer over the silver reduces the initial reflectance, but provides somewhat improved durability during salt fog exposure. Results from salt fog exposure of a mirror with a 100Å SiN_x protective layer over the silver are shown in Figure 12 and Figure 13. A reduced loss in reflectance is observed. However, a similar increase in scatter is measured, from 4.3×10^{-5}/sr pretest to 2.5×10^{-2}/sr, and significant degradation is evident visually. The initial increase in reflectance after 2 hr of salt fog exposure is likely due to the removal or agglomeration of the SiN_x overcoat layer to expose the silver underneath, which has higher reflectance. Subsequent degradation of the exposed silver after the additional 2 hr of salt fog exposure results in the reduced reflectance.

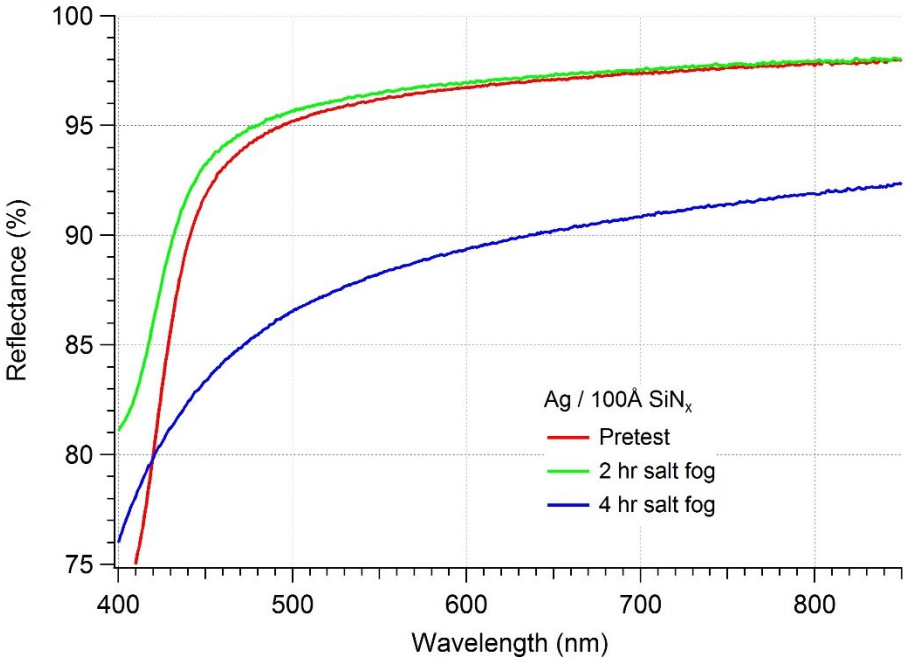

Figure 12. Reflectance spectra of a mirror with 100Å of SiN_x over Ag before and after salt fog exposure.

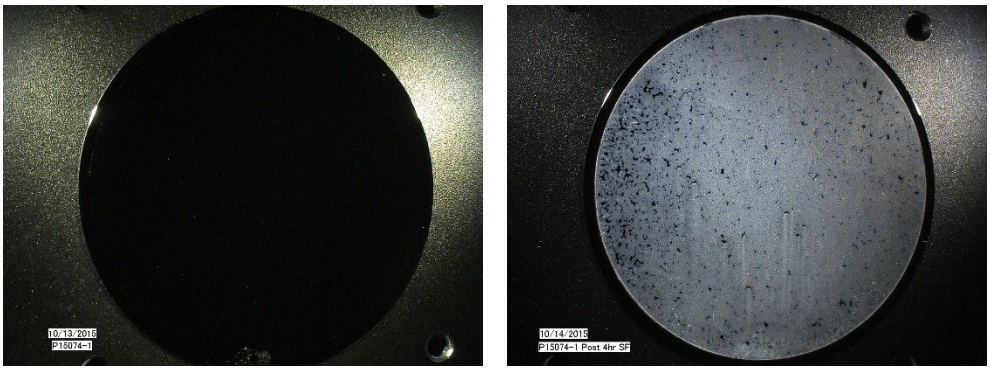

(a) (b)

Figure 13. Dark field images of a mirror with 100Å of SiN_x over Ag (a) before and (b) after 4 hr salt fog exposure.

The addition of a very thin adhesion layer between the silver and the 100Å SiN_x dielectric protection layer substantially increases mirror durability during salt fog exposure, though also further decreases the initial reflectance. Reflectance spectra for mirrors with three different thicknesses of a $NiCrN_x$ adhesion layer are shown in Figure 14. While these mirrors exhibit up to 10% reduced initial reflectance when compared to bare silver, no degradation is observed after 4

hours of salt fog exposure. Moreover, further salt fog exposure, up to 16 hr, shows no additional degradation in reflectance. In addition, minimal increases in measured scatter are observed from approximately 4×10^{-5}/sr pretest to 4.5×10^{-5}/sr after 4 hours of exposure, as evidenced in Figure 15. The $NiCrN_x$ adhesion layers dramatically improve mirror durability.

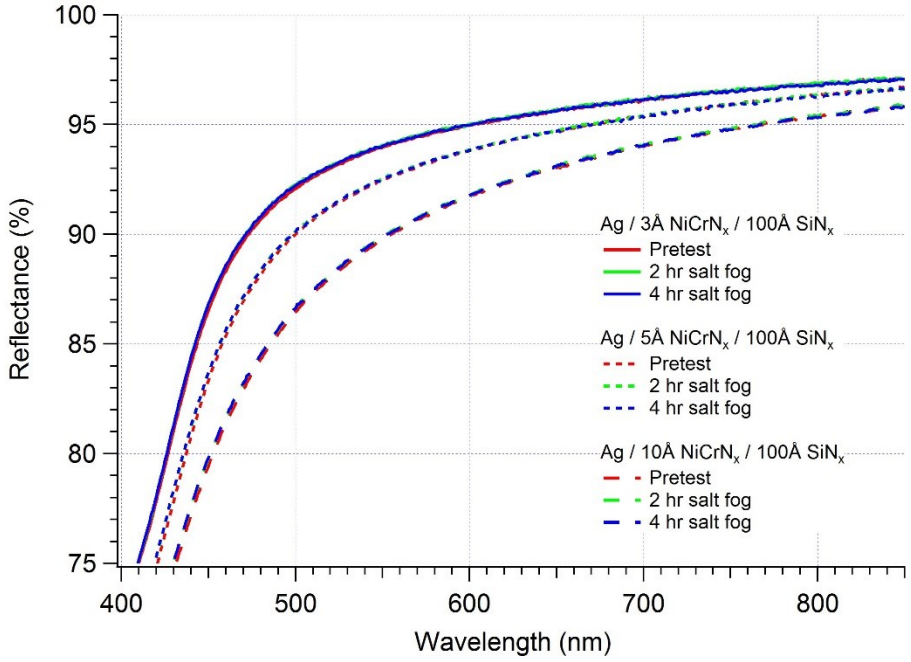

Figure 14. Reflectance spectra of mirrors with 100Å of SiN_x over thin $NiCrN_x$ over Ag before and after salt fog exposure.

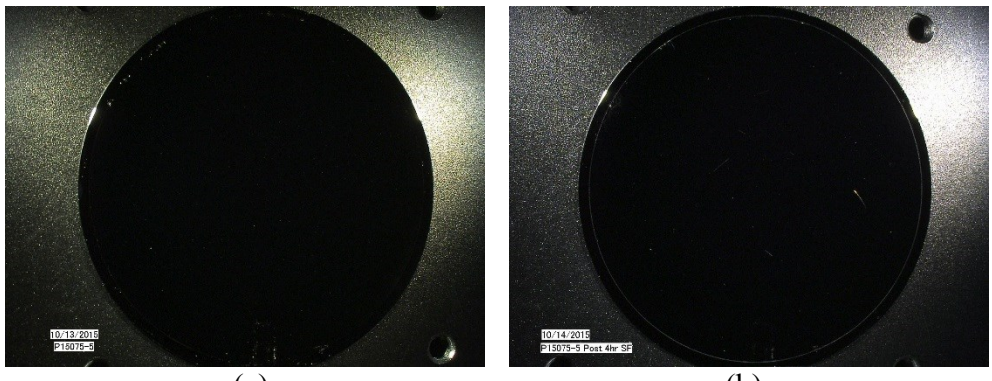

(a) (b)

Figure 15. Dark field images of a mirror with 100Å of SiN_x over 5Å $NiCrN_x$ over Ag (a) before and (b) after 4 hr salt fog exposure.

The results from salt fog exposure testing of these plasma beam sputtered silver mirrors correlate with previous testing of magnetron sputtered silver mirrors, as well as with testing of plasma beam sputtered silver mirrors with chromium adhesion layers [9, 11, 18]. While 100Å of SiN_x affords some protection to the silver, the thin adhesion layer is necessary to achieve robust mirror durability and maintain optical performance during salt fog exposure.

Interestingly, thin $NiCrN_x$ is not considered a protection layer on its own [9, 12]. Salt fog exposure of a plasma beam sputtered silver mirror topped with only 10Å of $NiCrN_x$ initially indicates increased reflectance, as shown in Figure 16. This is attributed to removal or agglomeration of the $NiCrN_x$ to expose the highly-reflective bare silver beneath, as mentioned previously for the mirror with 100Å SiN_x over Ag. It is expected that additional salt fog exposure will reduce the reflectance because the mirror has already begun to degrade, as evidenced by the measured scatter increasing nearly two orders of magnitude from 2.5×10^{-5}/sr pretest to 1.2×10^{-3}/sr after 4 hrs of salt fog exposure. Dark field images of the degraded mirror are shown in Figure 17.

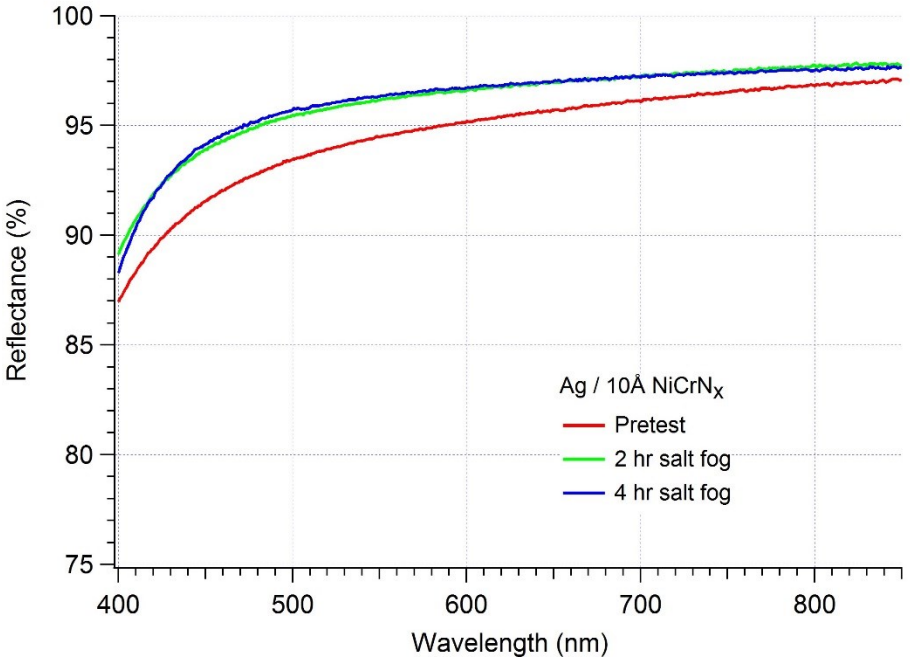

Figure 16. Reflectance spectra of a mirror with 10Å of $NiCrN_x$ over Ag before and after salt fog exposure.

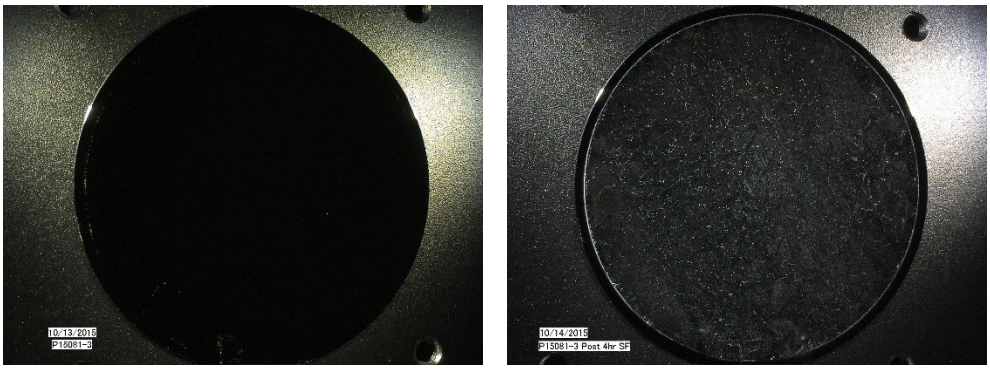

(a) (b)

Figure 17. Dark field images of a mirror with 10Å of $NiCrN_x$ over Ag (a) before and (b) after 4 hr salt fog exposure.

5.2 Mixed flowing gas exposure

While salt fog exposure has long been a standard test to assess mirror durability, MFG exposure has recently been considered a better analog for real long-term environmental exposure [19, 28, 29]. Initially, three protected silver mirror samples were tested in MFG exposure to compare two adhesion layer materials: CrN_x and $NiCrN_x$. The samples were tested for a total of 10 days (242 hr) in two to three day increments. Reflectance results from (1) a mirror with 100Å SiN_x over Ag, (2) a mirror with 100Å SiN_x over 5Å CrN_x over Ag, and (3) a mirror with 100Å SiN_x over 5Å $NiCrN_x$ over Ag are shown in Figure 18.

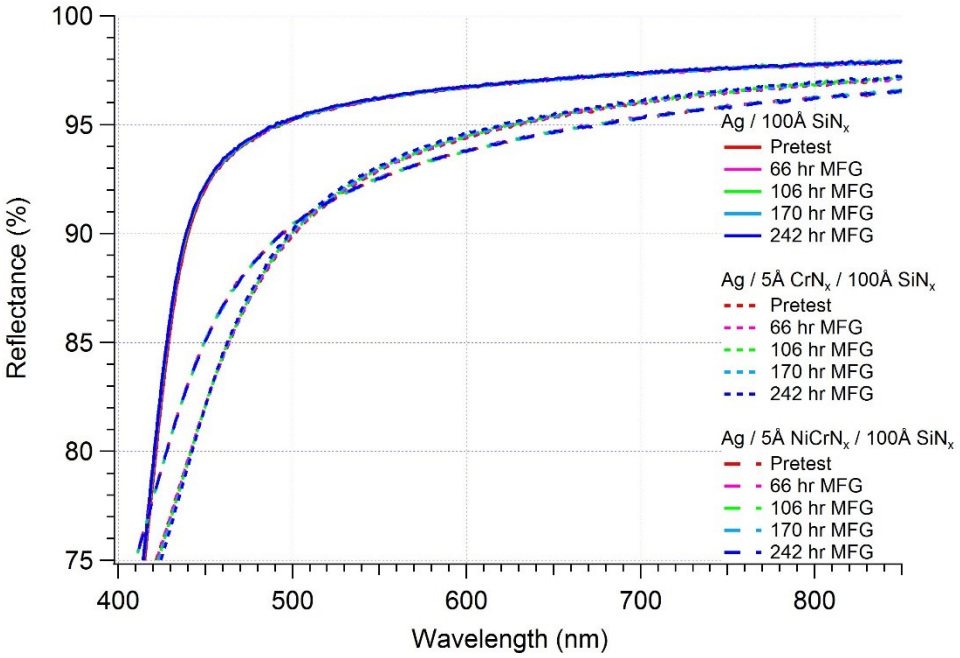

Figure 18. Reflectance spectra of silver mirrors with different adhesion layers before and after MFG exposure.

While no change in reflectance was observed at the center of any of the three mirrors, dark field images in Figure 19 indicate degradation has begun to occur. In particular, the mirror with no adhesion layer has begun to degrade significantly around the edge. In contrast, the mirror with the 5Å CrN_x adhesion layer is slightly degraded at the edge, while the mirror with the 5Å $NiCrN_x$ adhesion layer is only just beginning to degrade at the edge. All three mirrors show some degradation in the center, not enough to affect the measured reflectance, but enough to affect the measured scattered, as shown in Table 4.

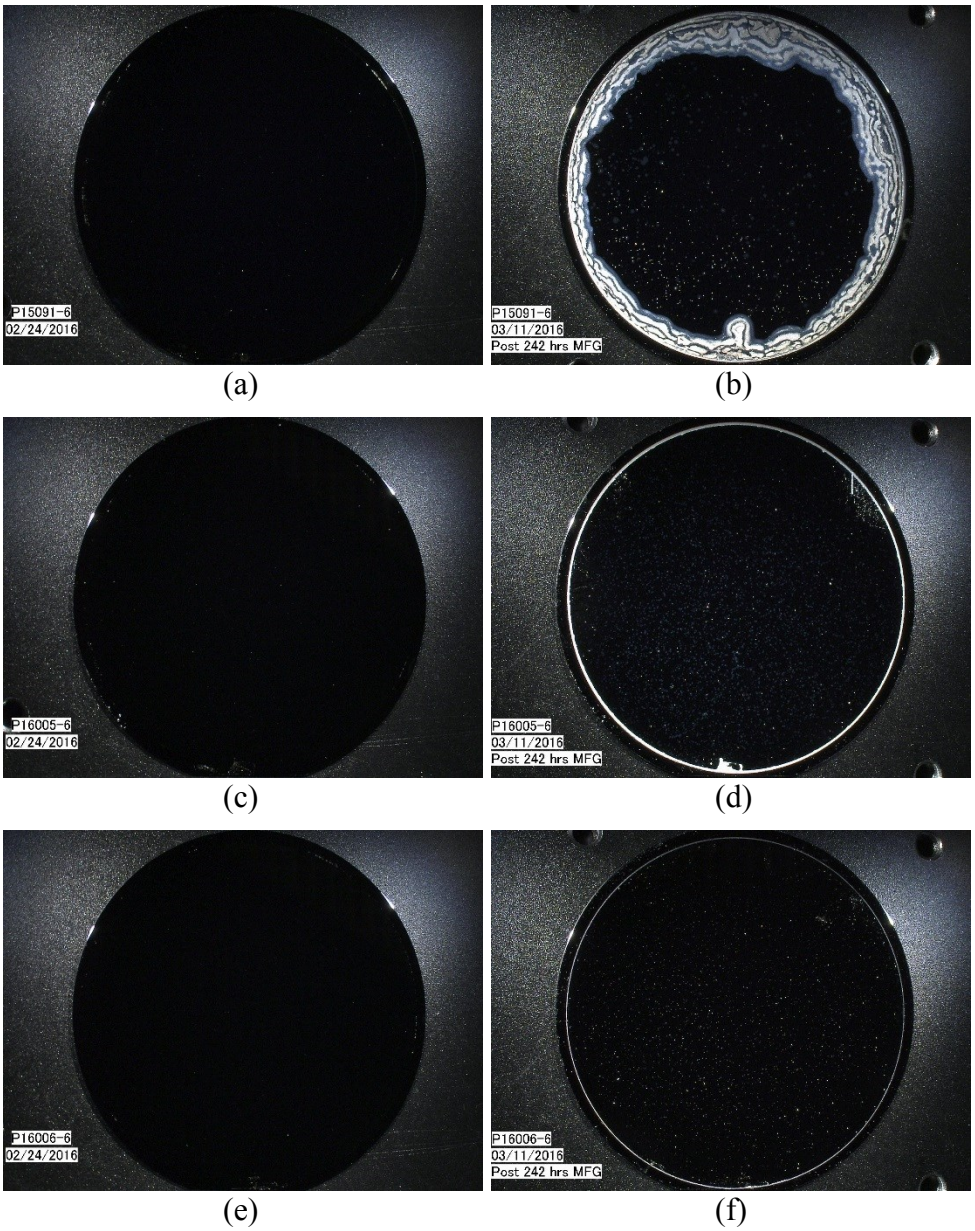

Figure 19. Dark field images of silver mirrors with different adhesion layers (a, c, e) before and (b, d, f) after 242 hr MFG exposure. (a, b) 100Å SiN_x over Ag, (c, d) 100Å SiN_x over 5Å CrN_x over Ag, and (e, f) 100Å SiN_x over 5Å $NiCrN_x$ over Ag.

Table 4. Scatter and Surface Roughness of Silver Mirrors Before and After MFG Exposure

	100Å SiN_x over Ag		**100Å SiN_x over 5Å CrN_x over Ag**		**100Å SiN_x over 5Å $NiCrN_x$ over Ag**	
	Pretest	242 hr MFG	Pretest	242 hr MFG	Pretest	242 hr MFG
BRDF (0,0)°, $\times 10^{-5}$	4.5	6.3	4.8	7.1	3.8	11.8
BRDF (50,180)°, $\times 10^{-5}$	2.3	2.8	2.3	3.5	2.1	3.5
Surface Roughness (Å)	4.5	5.5	4.7	5.8	4.3	7.9

Interestingly, it is the mirror with the 5Å $NiCrN_x$ adhesion layer that shows the largest increase in scatter and surface roughness, even though it visually appears the least degraded and previous research suggests that $NiCrN_x$ is an optimal adhesion layer [12]. Detailed characterization was performed on the exposed mirrors to investigate this corrosion behavior.

5.2.1 Optical microscopy

Optical micrographs of the corrosion features were obtained at two to three day intervals throughout MFG exposure. As shown in Figure 20, the mirror with no adhesion layer has corrosion features with large regions of small blisters surrounding central pinholes. There are no defined edges to the regions of blisters; rather, the blisters decrease in size and density as the distance from the center pinhole increases. The blister regions grow radially in size with time during MFG exposure as the reaction penetrates laterally into the coating layers. The central pinhole does not appear to change substantially with time.

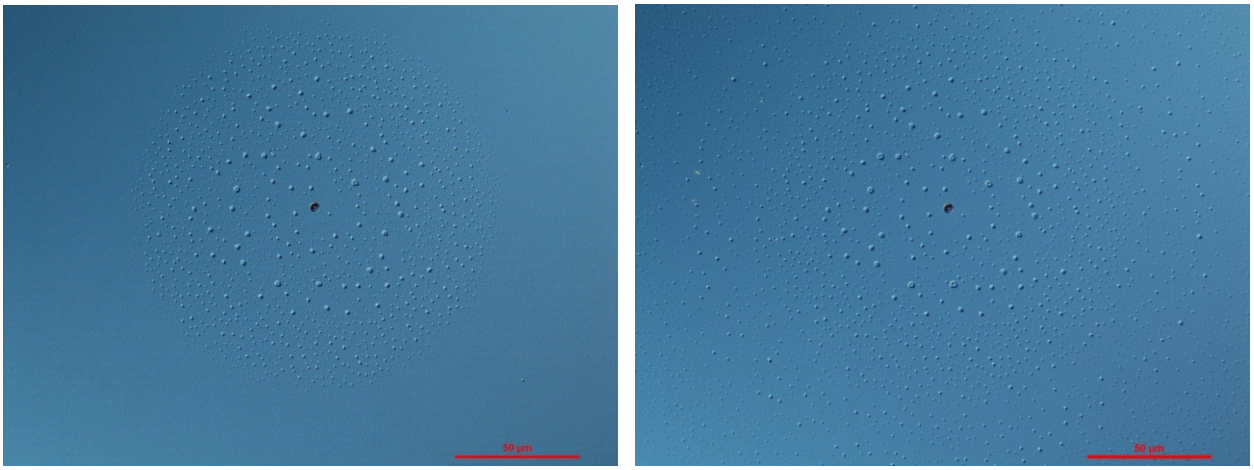

(a) (b)

Figure 20. Optical micrographs of a corrosion feature on 100Å SiN_x over Ag (a) after 66 hr and (b) after 242 hr MFG exposure.

Figure 21 and Figure 22 show corrosion features on the mirror with the 5Å CrN_x adhesion layer; arrows mark the outer edges. These corrosion features are large circular regions that also grow radially in size during exposure. Compared to the features on the mirror with no adhesion layer, these regions are more uniform, lack blisters, and have sharp, defined edges. In addition, the central pinholes in these features change with time, appearing to erupt somewhat. Figure 22 shows better detail of the center, as well as the edge and the ring-like growing front. The adhesion layer has changed the lateral mechanism of corrosion.

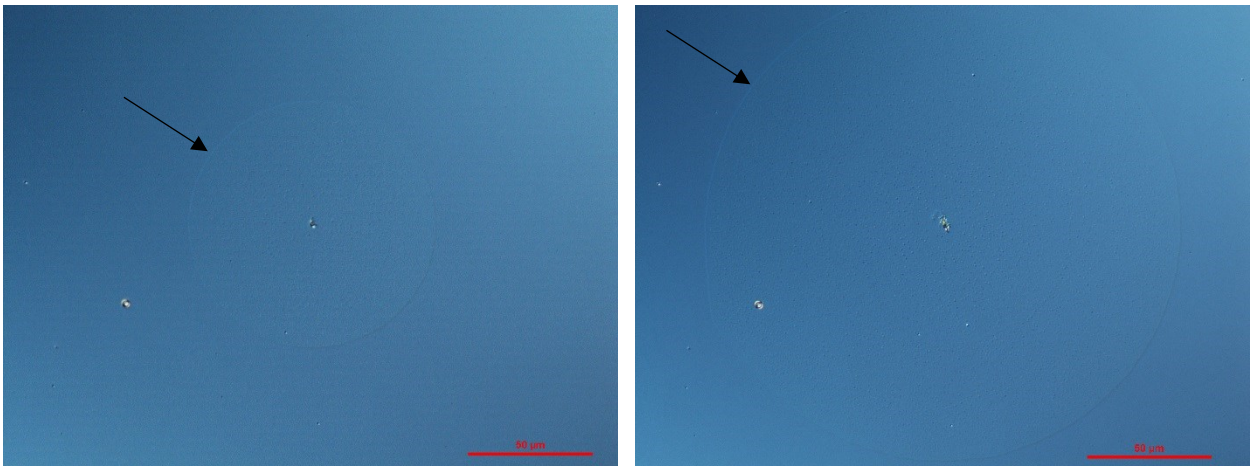

(a) (b)

Figure 21. Optical micrographs of a corrosion feature on 100Å SiN_x over 5Å CrN_x over Ag after (a) 66 hr and (b) 170 hr MFG exposure.

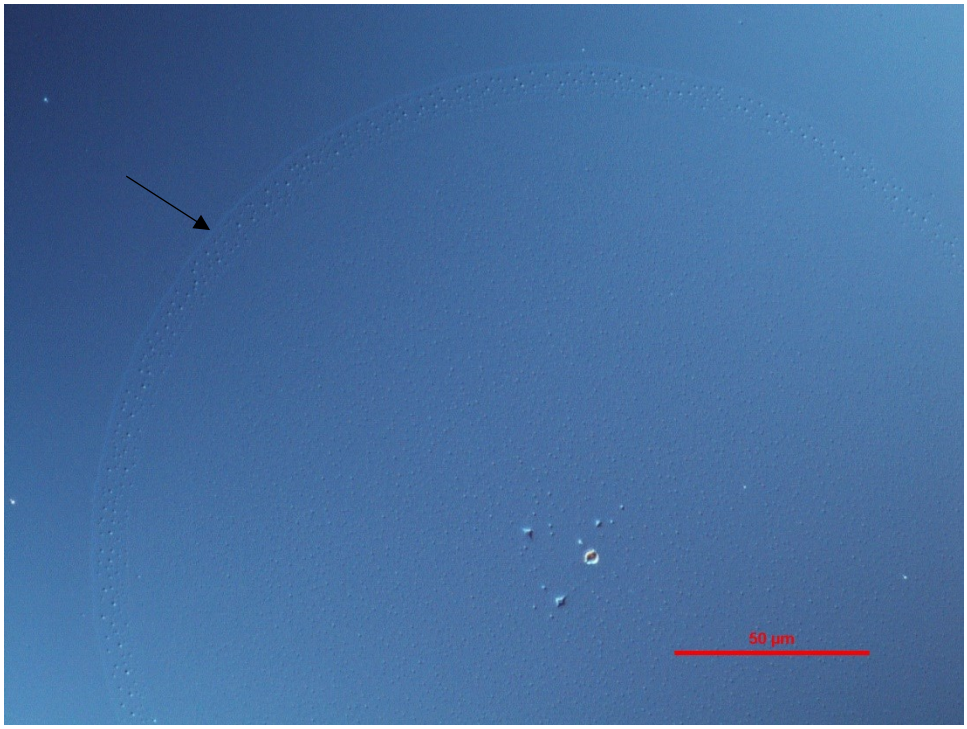

Figure 22. Optical micrograph of a different corrosion feature on 100Å SiN_x over 5Å CrN_x over Ag after 242 hr MFG exposure.

For the mirror with the 5Å $NiCrN_x$ adhesion layer, Figure 23 and Figure 24 show corrosion features that differ substantially from the previous two mirrors. The features are overall significantly smaller in size. Moreover, they have relatively large central eruptions and much

smaller surrounding circular regions that do not grow substantially with time. However, the eruption centers are changing significantly with time, growing in size and irregularity.

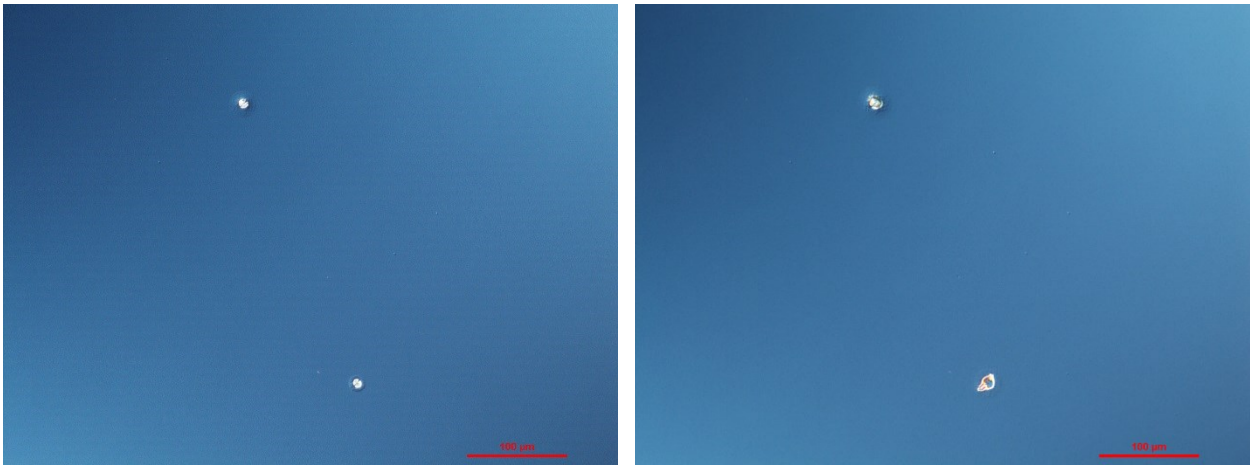

(a) (b)

Figure 23. Optical micrographs of corrosion features on 100Å SiN_x over 5Å $NiCrN_x$ over Ag after (a) 106 hr and (b) 242 hr MFG exposure.

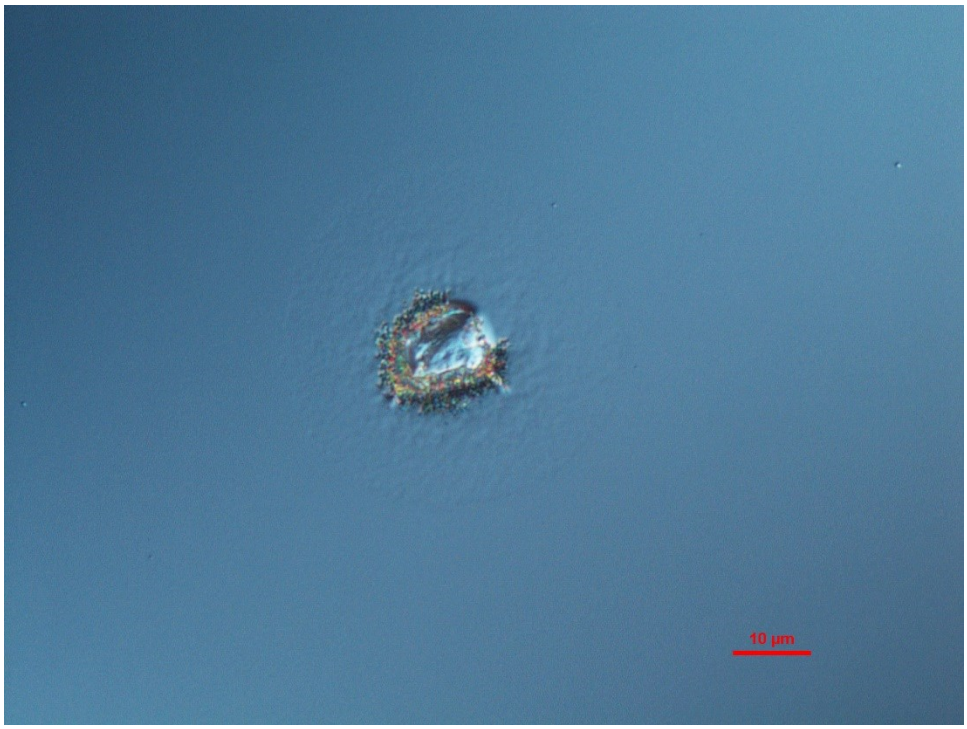

Figure 24. Optical micrograph of a different corrosion feature on 100Å SiN_x over 5Å $NiCrN_x$ over Ag after 242 hr MFG exposure.

5.2.2 Scanning electron microscopy

For more detailed investigation, scanning electron micrographs were taken of the corrosion features on each of the three mirrors after 242 hr of MFG exposure. Figure 25 and Figure 26 show a corrosion feature on the mirror with no adhesion layer. The blisters are clearly evident and believed to be occurring at the Ag-SiN_x interface. Compared to the optical micrographs, the circular region of blisters shows a more clearly defined edge. This topographical contrast suggests that changes are occurring within the layered structure in this region. However, EDS data are inconclusive on whether this region has experienced significant compositional changes. The white spots at the blister region edge appear slightly richer in silver, suggesting atomic migration has resulted in subsurface silver agglomeration, which may be the cause of the blisters. It is not clear if the tiny dark spots in the backscatter image are silver voids. Additionally, the EDS data do not show significant corrosion products. The central feature appears as an eruption that has not yet fully broken open; EDS data indicate it is predominantly silicon. This suggests either the SiN_x material is agglomerated and protruding at the center, preventing detection of the layers beneath; or, a pinhole exists below the central feature extending through the coating layers to the silicon substrate beneath. Besides the central feature which may penetrate the coating layers, there is no evidence of significant breaks in the protective SiN_x layer, which appears intact throughout the blister region. Ultimately, changes are occurring within the coating layers, indicating that lateral migration of silver is an important factor in the corrosion process.

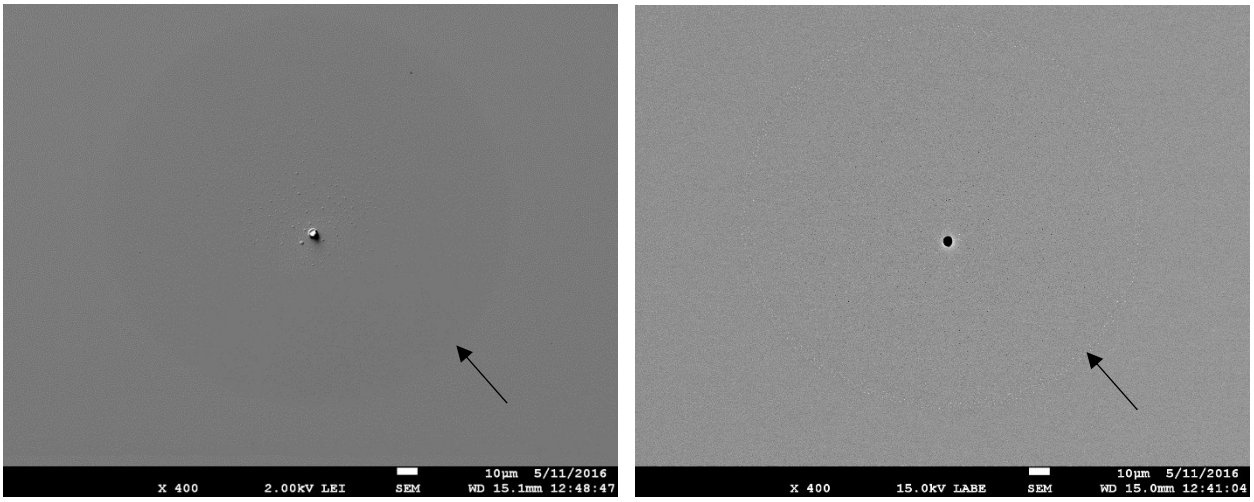

(a) (b)

Figure 25. SEM micrographs of a corrosion feature on 100Å SiN_x over Ag after 242 hr MFG exposure. Micrographs obtained in (a) secondary electron mode at 2kV and in (b) backscatter electron mode at 15 kV.

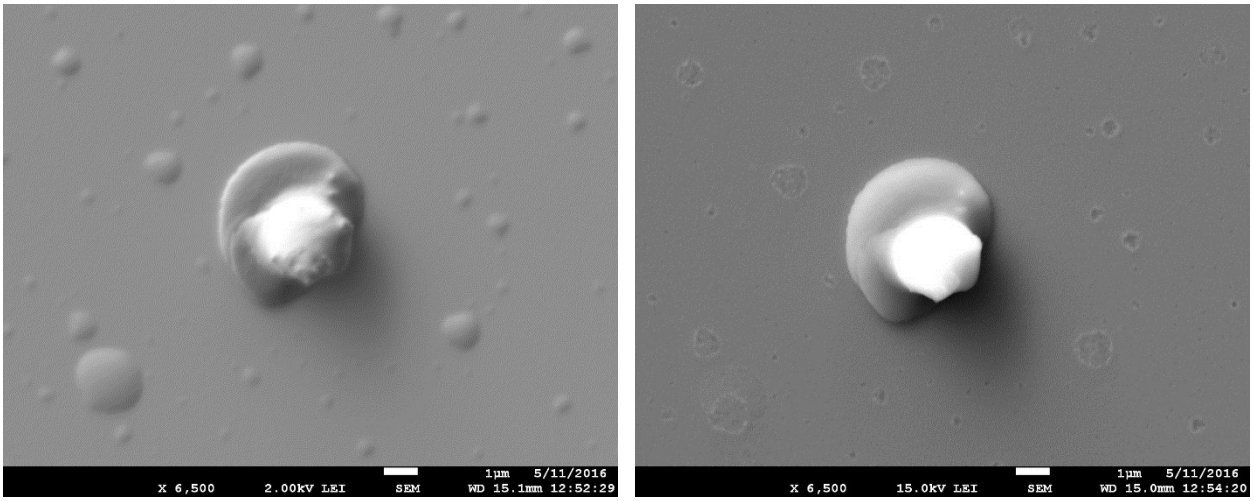

(a) (b)

Figure 26. SEM micrographs of the center of a corrosion feature on 100Å SiN_x over Ag after 242 hr MFG exposure. Micrographs obtained with an accelerating voltage of (a) 2 kV and (b) 15 kV.

SEM micrographs of a corrosion feature on the mirror with the 5Å CrN_x adhesion layer are shown in Figure 27. These corrosion features show similar large circular diffusion regions, but with more obvious small agglomerates of silver and regions of silver depletion. However, as with the mirror with no adhesion layer, the small size of the agglomerates and the limited topographical

contrast in Figure 27a suggests that the amount of atomic migration is relatively small. Large voids, significant silver depletion, and sizable silver agglomeration are not observed. Even so, the radial sizes of these circular diffusion regions are quite large, again suggesting that subsurface silver migration is an important factor in the corrosion process. It is not clear from these images where in the silver layer this migration is occurring. Finally, blisters are not observed, suggesting that while silver migration is evident, the Ag-CrN_x-SiN_x interface is better adhered than the Ag-SiN_x interface in the mirror with no adhesion layer.

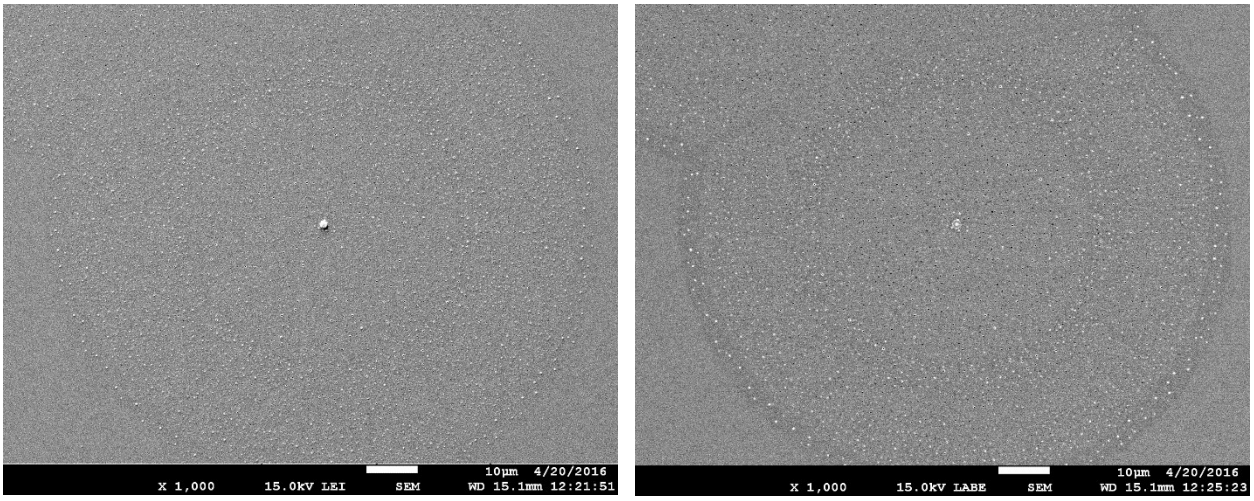

(a) (b)

Figure 27. SEM micrographs of a corrosion feature on 100Å SiN_x over 5Å CrN_x over Ag after 242 hr MFG exposure. Micrographs obtained in (a) secondary electron mode and (b) backscatter electron mode.

The concentric rings within the circular diffusion region correspond to the two to three day increments of MFG exposure. Results from MFG exposure testing conducted under the same test conditions for 10 continuous days with no stopping do not show the same types of ring features. While periodically stopping the MFG exposure for analysis must be changing the dynamics of the corrosion process, it is not entirely clear why these rings form.

While the central feature in Figure 27 appears similar to that of the mirror with no adhesion layer, Figure 28 shows the central area of a different corrosion feature on the CrN_x adhesion layer

mirror. Here, the eruption has broken open and significant corrosion is evident. The white crystallites are predominately silver, though chlorine and sulfur are also detected. The sulfur signal is particularly strong at the spikey feature in the center of the image, suggesting that silver sulfide whiskers have formed [7, 8]. The black regions immediately surrounding the silver agglomerates show virtually no silver. The dark gray regions around the black regions further indicate silver depletion; chlorine is also detected in the dark gray regions. Previous researchers have observed similar morphological features in the corrosion of protected silver mirrors [10, 11]. Silver agglomeration is occurring at the expense of the surrounding silver layer, suggesting that lateral silver migration, and not just silver corrosion, is an important factor in the corrosion process.

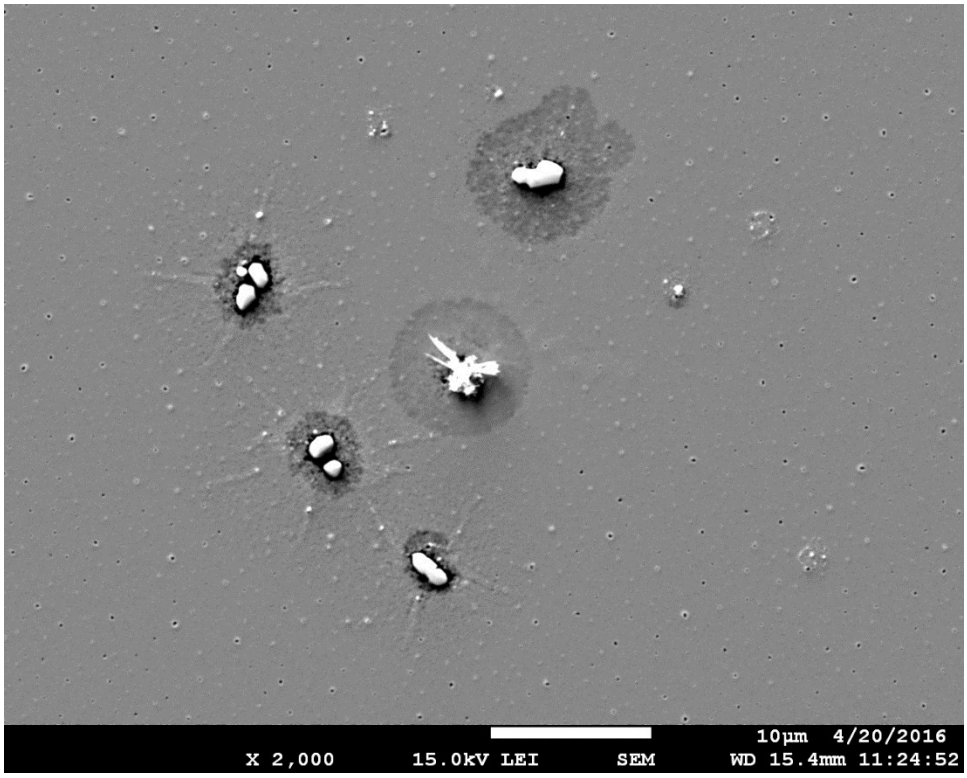

Figure 28. SEM micrograph of the center of a different corrosion feature on 100Å SiN_x over 5Å CrN_x over Ag after 242 hr MFG exposure.

It should be mentioned that the limited amount of chlorine detected in the corrosion features on all three mirrors does not necessarily indicate the absence of chlorine in the corrosion

process. AgCl is known to undergo photo-reduction into metallic Ag [11, 19]. It is possible that Cl_2 gas reacted with silver during MFG exposure, resulting in the formation of AgCl particles that were reduced to Ag particles due to exposure to fluorescent room lights during and after testing.

SEM micrographs of a corrosion feature on the mirror with the 5Å $NiCrN_x$ adhesion layer are shown in Figure 29 and Figure 30. While the corrosion features on this mirror are significantly smaller than those on the previous mirrors, they display many similar types of features. The circular diffusion region shows areas of silver depletion with a central silver agglomerate. Immediately surrounding the silver agglomerate are large void regions that are nearly entirely depleted of silver; these are the darkest gray regions in Figure 29. Chlorine was again detected in the regions near the central silver agglomerate. In addition, sulfur, chlorine, oxygen, nitrogen, and phosphorous were detected at the silver agglomerate, particularly in the dark region on top of the lower left portion of the agglomerate (see arrows in Figure 30). The corrosion process here is clearly complicated. The presence of sulfur, chlorine, oxygen, and nitrogen is understood in light of the MFG exposure. The appearance of phosphorous is not well-understood and may either be an impurity or surface contamination prior to MFG exposure.

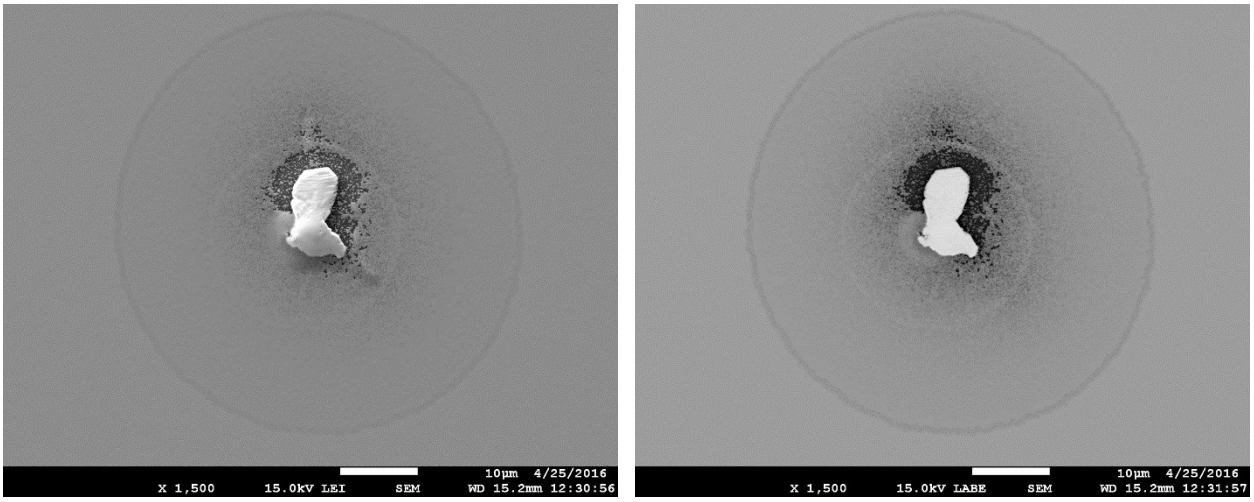

(a) (b)

Figure 29. SEM micrographs of a corrosion feature on 100Å SiN_x over 5Å $NiCrN_x$ over Ag after 242 hr MFG exposure. Micrographs obtained in (a) secondary electron mode and (b) backscatter electron mode.

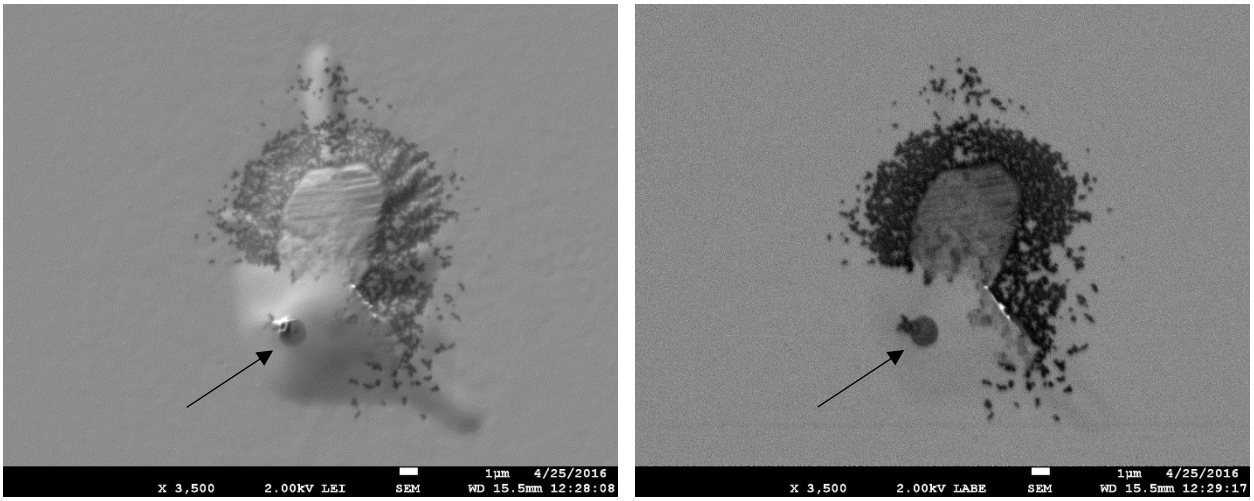

(a) (b)

Figure 30. SEM micrographs of the center of a corrosion feature on 100Å SiN_x over 5Å $NiCrN_x$ over Ag after 242 hr MFG exposure. Micrographs obtained with an accelerating voltage of 2 kV in (a) secondary electron mode and (b) backscatter electron mode.

The images in Figure 30 of the center of the corrosion feature were taken at an accelerating voltage of 2 kV. Under this condition, the very surface of the coating is probed in greater detail. It appears that the SiN_x layer is at least partially intact over the silver agglomerate (see arrows). In fact, the unusual topography in Figure 30a, and the unexpected contrast in the backscatter image

in Figure 30b, suggest that the SiN_x layer may be intact over the entire silver agglomerate. This would imply that the silver migration occurs below the protective SiN_x layer, and that the small dark region of material with the large signal of corrosion products is actually on top of the SiN_x layer. It is likely that only small pores or breaks in the SiN_x layer drive the corrosion process.

5.2.3 Cross-sectional TEM: $NiCrN_x$ adhesion layer mirror

Cross-sectional TEM was used to further analyze the corrosion features on the mirror with the 5Å $NiCrN_x$ adhesion layer. SEM images of the corrosion feature were obtained during FIB sample preparation and are shown in Figure 31. While this is not the exact feature imaged in Figure 29 and Figure 30, it shows similar aspects of silver agglomeration at the expense of silver depletion from the surrounding area. It also shows at least a partially-intact SiN_x layer over the agglomerate and the surrounding voids, as well as regions of other material present on top of the agglomerate.

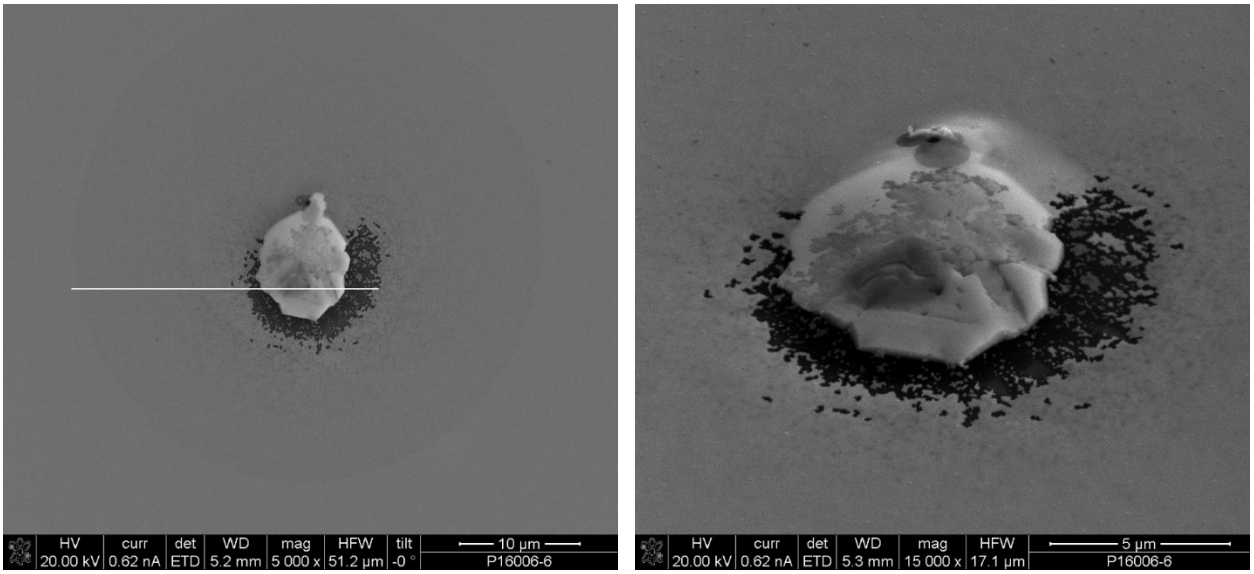

(a) (b)

Figure 31. SEM micrographs during FIB of a corrosion feature on 100Å SiN_x over 5Å $NiCrN_x$ over Ag after 242 hr MFG exposure. Micrograph obtained (a) top-down and (b) at an angle to view topography.

An overview of the entire TEM specimen is shown in Figure 32; it approximately corresponds to the white line in Figure 31. The length of the TEM specimen was chosen to investigate the circular diffusion region surrounding the central silver agglomerate to fully understand the role of lateral silver migration in the corrosion process. The cross-section location on the corrosion feature was chosen to investigate the dark region of corrosion products on top of the silver agglomerate. A detailed image of the central silver agglomerate is shown in Figure 33.

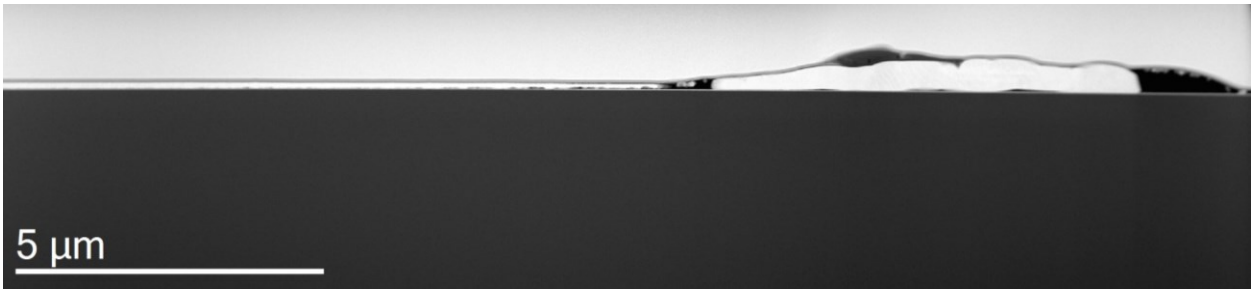

Figure 32. HAADF overview image of the TEM specimen taken from the corrosion feature on 100Å SiN_x over 5Å $NiCrN_x$ over Ag after 242 hr MFG exposure.

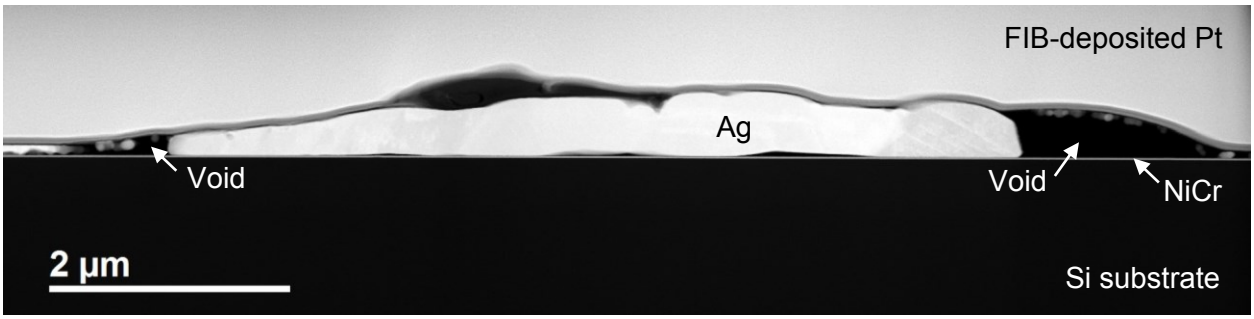

Figure 33. HAADF image of the central silver agglomerate of the corrosion feature.

These images correspond well to the phenomena observed in the SEM. Far from the central silver agglomerate, the coating appears intact; the silicon substrate is smoothly coated with the mirror stack. Nearer to the center of the corrosion feature, the bottom of the silver layer is no longer intact and depletion of silver has begun. At the center of the corrosion feature, the silver has agglomerated, leaving behind large voids depleted of silver. The void regions labeled in Figure 33 correspond to the darkest gray regions in Figure 31. The central agglomerate is almost entirely

silver, with a very small EDS signal of chlorine. Figure 34 and Figure 35 show detailed images of the lateral silver migration from the base of the Ag layer to the agglomerate. The small particles in the void region are silver; no corrosion products are detected.

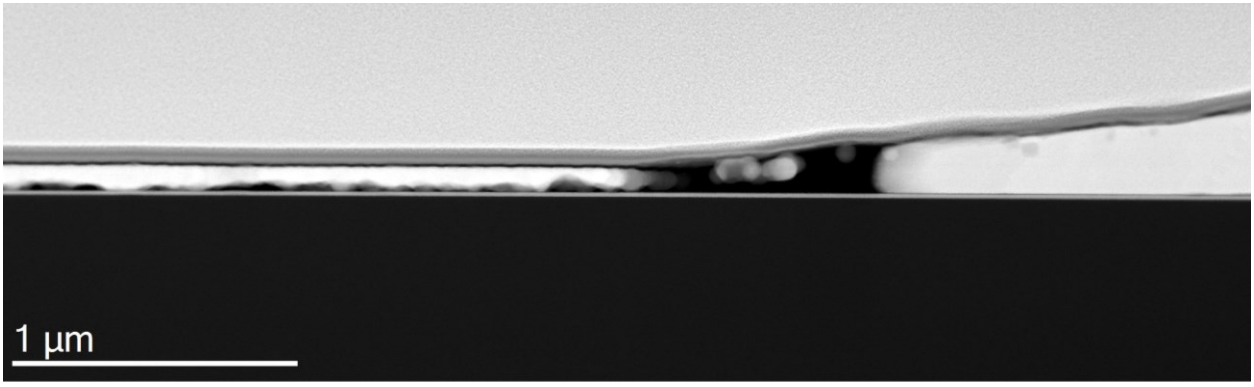

Figure 34. HAADF image of voids and depletion in the Ag layer. Left side of center.

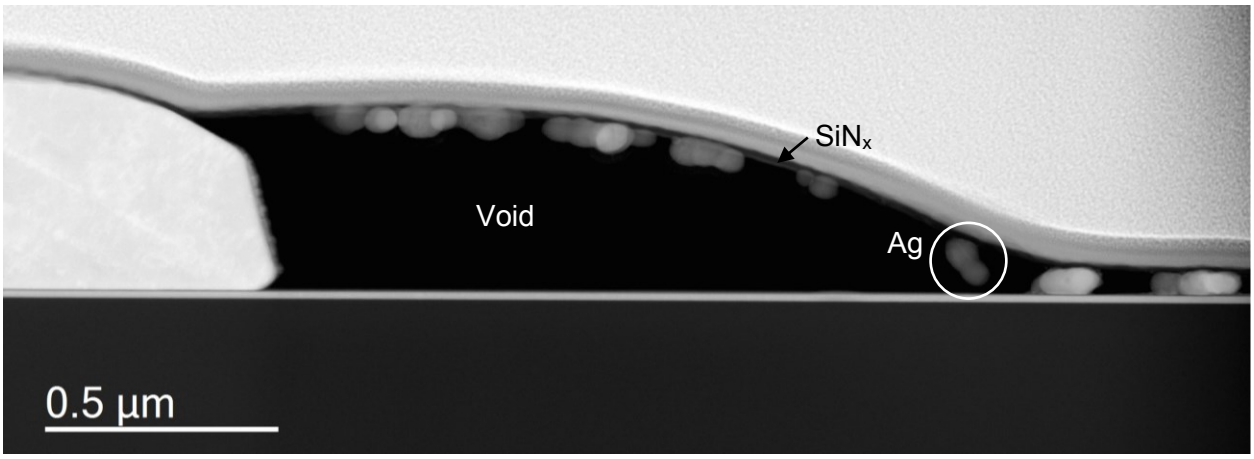

Figure 35. HAADF image of voids and depletion in the Ag layer. Right side of center.

Close inspection of the above images suggests that the SiN_x layer is intact across most, if not all, of the corrosion feature. The SiN_x layer is the thin, dark gray layer that follows the top of the silver and the bottom of the FIB-deposited platinum. Figure 35 and Figure 36 clearly show the intact SiN_x layer at the edge of the silver depletion region extending across the voids created by the agglomerated silver. This corresponds to the low-voltage SEM micrographs that also showed this layer was at least partially-intact above the silver agglomerate.

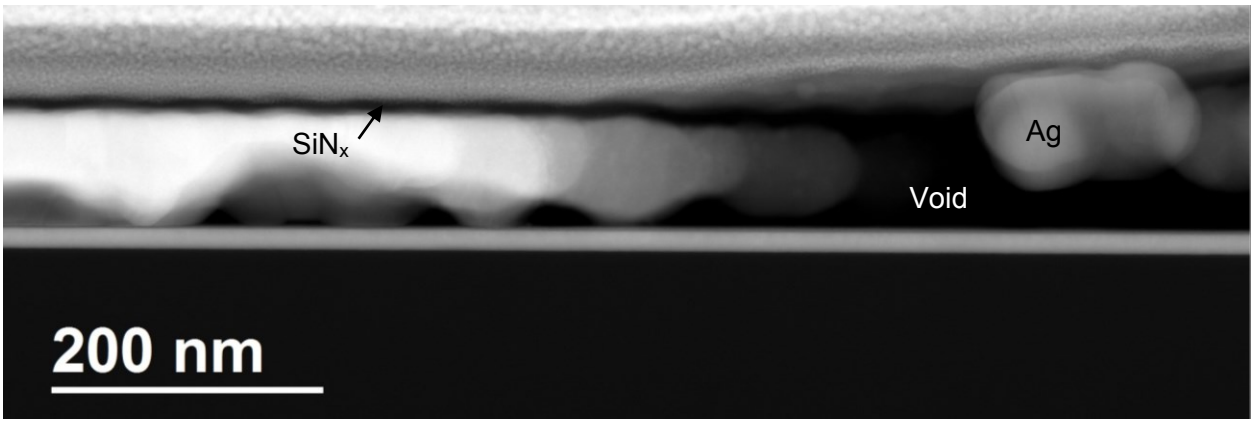

Figure 36. HAADF image of the Ag layer where silver depletion begins.

The depletion of silver from the base of the Ag layer is causing the layer to thin, to the extent that voids are created between the NiCr and the SiN_x layers, and the distance between those layers is decreased. Figure 37 shows images of this thinning by comparing the mirror coating layers far from the agglomerated silver (a) and near to it (b). Interestingly, the NiCr layer is also thinning near to the agglomerated silver. Approximate average thickness measurements of the Ag and NiCr layers in the two regions are shown in Table 5. The SiN_x layer appears the same in the two regions and has not thinned. EDS maps also indicate that the thin 5Å $NiCrN_x$ adhesion layer appears generally the same as well. Atomic migration is occurring only from the lower two layers.

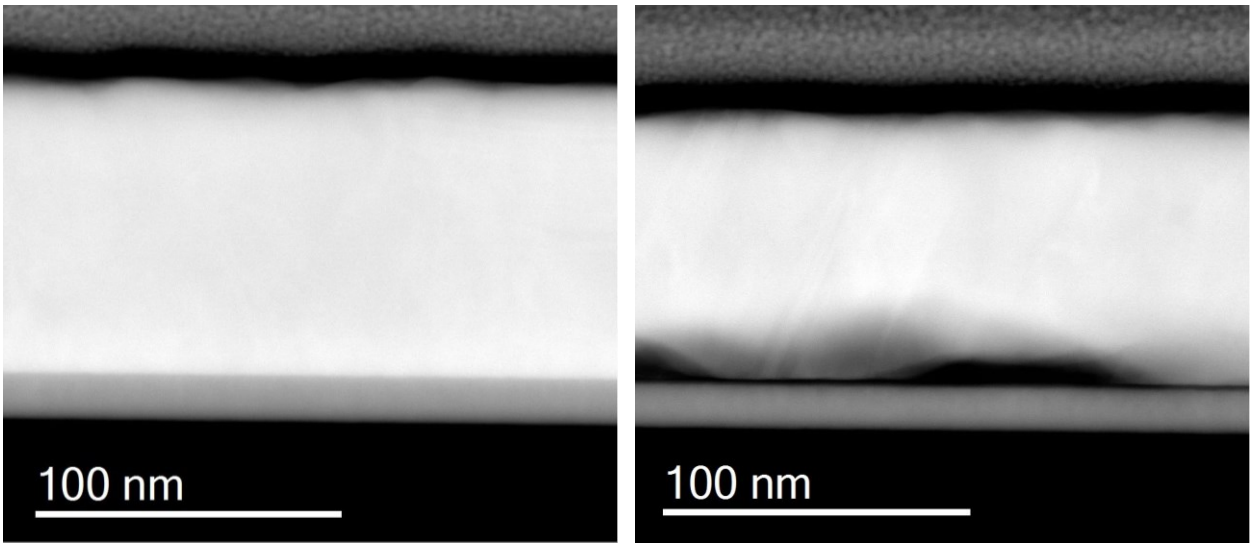

(a) (b)

Figure 37. HAADF images of the full mirror stack (a) far from the central silver agglomeration and (b) near to it.

Table 5. Approximate Layer Thickness in the Corrosion Feature

Layer	Average Thickness (Å)	
	Far from center Figure 37(a)	Near center Figure 37(b)
Ag	960	860
NiCr	150	130

To investigate the dark region of corrosion products above the silver in Figure 33, an ADF image is shown in Figure 38 and EDS maps of the portion in the white square are shown in Figure 39. The EDS maps clearly show the sharp distinction between the Ag layer, the SiN_x layer, and the material above, which has a large signal of nickel. The maps also show the presence of the 5Å $NiCrN_x$ adhesion layer between the Ag and the SiN_x. Further EDS analyses indicate that the silver agglomerate is predominately silver and that the SiN_x layer appears intact across the silver agglomerate. The material above the SiN_x has signals of nickel, chlorine, oxygen, carbon, and phosphorous; it has only a very small signal of silver. While the nickel likely came from the thinning NiCr layer underneath the Ag layer, how exactly it migrated above the SiN_x layer is not

immediately clear. A break in the SiN_x layer is not evident in this TEM specimen; it must be elsewhere on the corrosion feature or is too small to observe. The phosphorous signal corresponds with EDS data obtained in the SEM.

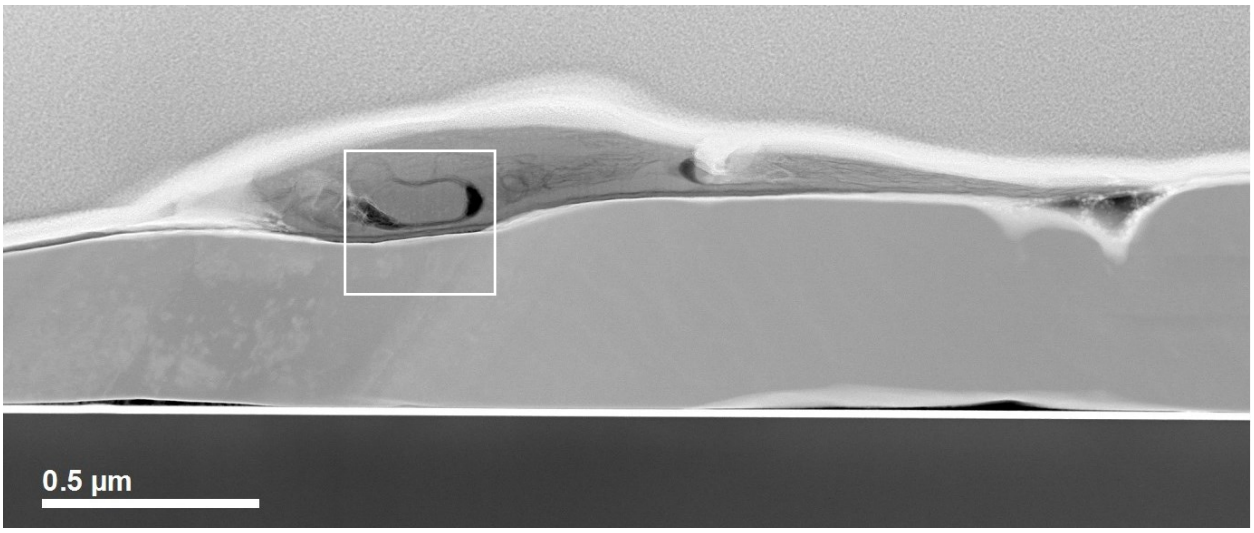

Figure 38. ADF image of the center of the corrosion feature with better detail of the material above the silver.

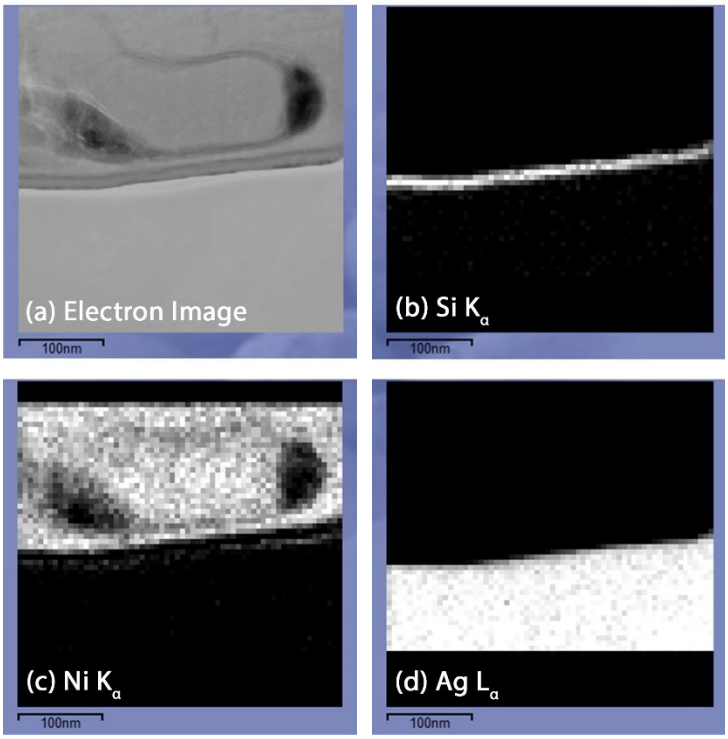

Figure 39. EDS maps of (b) Si, (c) Ni, and (d) Ag in a portion of the central corrosion feature (a).

Ultimately, the TEM data illustrate the importance of the lateral migration of silver during the corrosion process. The silver is being depleted from the base of its layer and agglomerated at the center of the corrosion feature. The limited sulfur, chlorine, and oxygen in the silver agglomerate suggests that the driving force for silver migration may not be the corrosion of silver itself. The nickel is also migrating and being depleted from the NiCr base layer; its appearance above the SiN_x layer along with significant corrosion products suggests its migration is driven by a corrosion potential. An electrochemical potential drives the nickel to react or corrode more readily than the silver. The nickel acts as a sacrificial corrosion material, thereby limiting corrosion of the silver. The silver migration and agglomeration is a byproduct of the nickel corrosion reaction.

The adherence of the top of the Ag layer to the SiN_x layer is explained by the 5Å $NiCrN_x$ adhesion layer. The thin $NiCrN_x$ layer promotes adhesion between the Ag and SiN_x, thereby preventing corrosion or atomic migration at that interface. This is supported by the XPS depth profiles presented in Section 4 that show nickel extending further into the silver layer than expected, thereby improving adhesion. While it is not clear from the XPS data the exact nature of the nickel-silver interaction at the Ag-$NiCrN_x$-SiN_x interface, the interface is clearly well-adhered since silver depletion does not occur there. The silver is preferentially depleted from the bottom of the silver layer at the NiCr-Ag interface, indicating that must be the weaker interface. Atomic migration along the NiCr-Ag interface could potentially be slowed if better adhesion at that interface could be achieved. How that would change the dynamics of the corrosion process is under investigation.

Finally, the TEM images further explain the increased scatter observed in the 5Å $NiCrN_x$ adhesion layer mirror after MFG exposure (see Table 4). The silver agglomerate is radially small

in size; however, the height of the agglomerate is approximately four times the initial coating height, as shown in Figure 32. This protrusion above the coating surface acts like a particle to scatter light. Many of these corrosion features across the mirror surface increase the observed scatter and surface roughness [10]. Over time, these scatter sites would lead to reduced reflectance if allowed to grow in size, number, and density through additional exposure and corrosion.

5.2.4 Cross-sectional TEM: CrN_x adhesion layer mirror

To compare the corrosion behavior of the different adhesion layer materials, a corrosion feature on the mirror with the 5Å CrN_x adhesion layer was also cross-sectioned for analysis. An overview of the TEM specimen is shown in Figure 40; a problem with the TEM software prevented the scale bar from being saved in this and subsequent images. Due to the large radial size of the corrosion features on the CrN_x adhesion layer mirror, only the central portion of the circular diffusion region could be included in the TEM specimen.

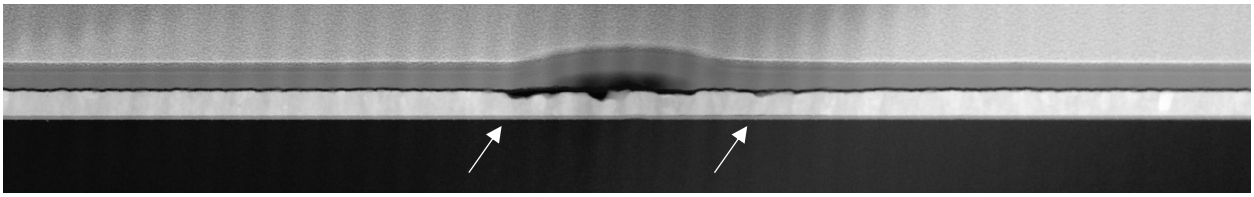

Figure 40. TEM image of the center of a corrosion feature on 100Å SiN_x over 5Å CrN_x over Ag after 242 hr MFG exposure.

Significant differences are readily apparent in the layered nanostructure of the corrosion features from the mirrors with the different adhesion layer materials. In the mirror with the CrN_x adhesion layer, the amount of silver migration is reduced. Notably, the silver depletion occurs at the top of the Ag layer, not at the bottom, as in the $NiCrN_x$ adhesion layer mirror. The resulting silver voids are small, and do not penetrate through the entire Ag layer thickness to the NiCr layer below. In addition, the largest voids are concentrated at the center of the corrosion feature and

there is no central silver agglomeration. The center of the corrosion feature is raised, though not nearly as much as in the corrosion feature on the $NiCrN_x$ adhesion layer mirror. This supports the larger increase in scatter and surface roughness observed for the $NiCrN_x$ adhesion layer mirror compared to the CrN_x adhesion layer mirror (see Table 4). It was not possible to analyze the composition of the material in the central region of this corrosion feature with EDS, though the raised feature does not appear to be silver, as indicated by the contrast in Figure 40.

It was also not possible to identify the presence of corrosion products in this sample or to perform measurements of layer thickness and depletion due to issues with instrument functionality and availability. Two subsequent images were obtained, corresponding to the locations indicated by the arrows in Figure 40; these images are shown in Figure 41 and Figure 42.

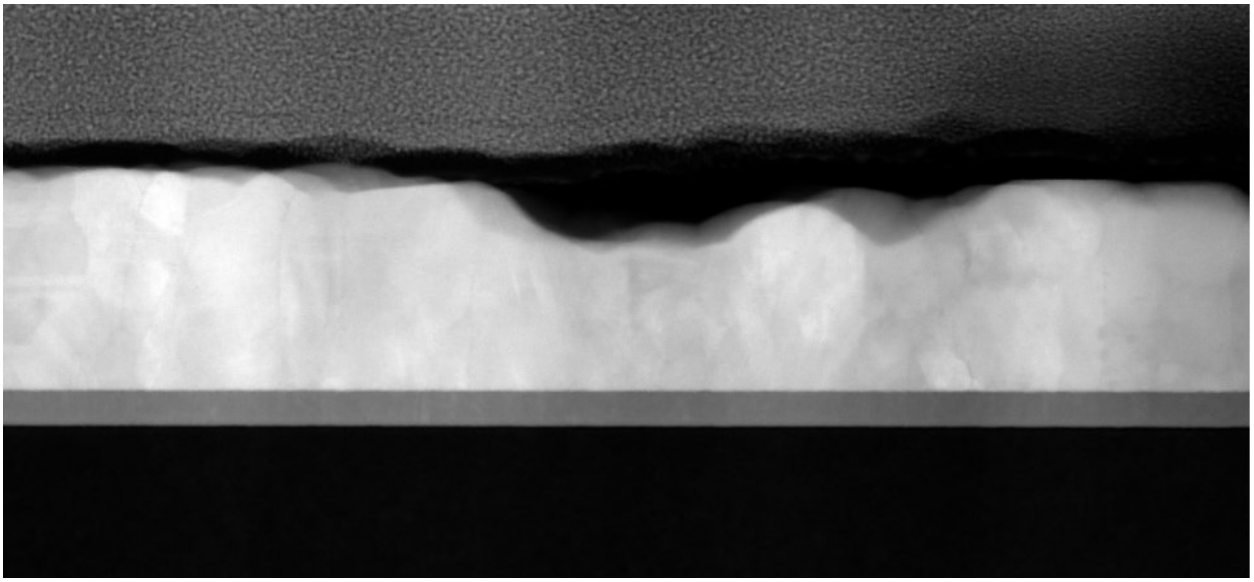

Figure 41. TEM image of depletion at the top of the Ag layer. Left side of center.

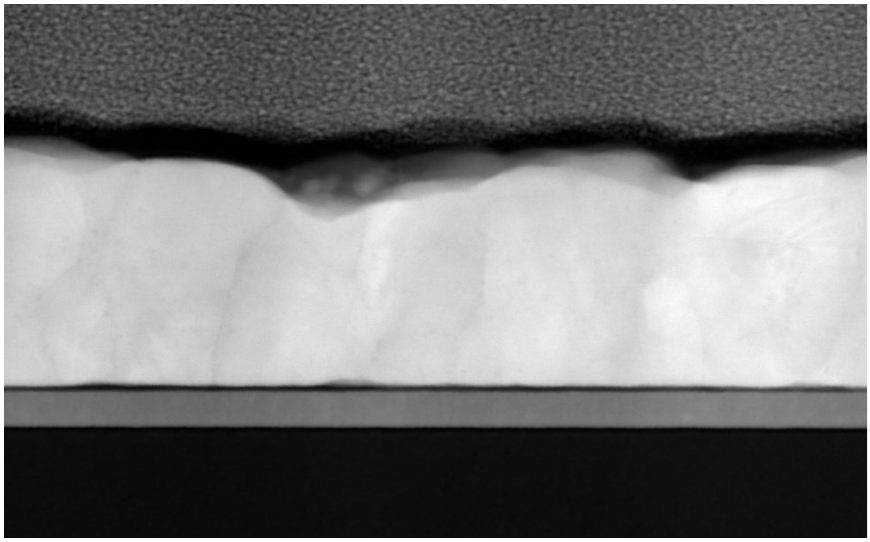

Figure 42. TEM image of depletion at the top of the Ag layer. Right side of center.

The small amount of silver migration shown in these images corroborates the earlier optical and SEM micrographs of the CrN_x adhesion layer mirror. In those images, low contrast in the circular diffusion regions compared to the regions outside of the corrosion features suggested that only a small amount of silver was migrating. While silver migration is occurring over a large area, as evidenced by the large radial size of the circular diffusion regions, the migration does not involve material from the full thickness of the silver layer. There is depletion and voiding only at the top of the layer. Compositional analyses and thickness measurements will elucidate the structure of these diffusion regions and the nature of the atomic migration.

Closer analysis of Figure 42 indicates a small gap between the bottom of the Ag layer and the NiCr layer below. In contrast, the region in Figure 41 appears well-adhered, with no apparent gap. It is not clear from these images if this gap is the result of silver depletion driven by the corrosion reaction or if the layers simply lost adhesion due to the corrosion dynamics. In the $NiCrN_x$ adhesion layer mirror, significant atomic migration was observed at this interface. Additional analyses of the CrN_x adhesion layer mirror will provide insight on whether that is also

occurring here. Regardless of the mechanism, the NiCr-Ag interface is clearly an important factor in the corrosion process.

In addition, it is evident that the absence of a small amount of nickel in the adhesion layer significantly affects the corrosion process. The voiding and silver depletion at the top of the Ag layer indicates the Ag-CrN_x-SiN_x interface is not as well-adhered as the Ag-$NiCrN_x$-SiN_x interface. The nickel serves to enhance adhesion at this interface, pinning the layers together and preventing atomic migration. The adhesion layer material must affect the electrochemical potential at the top of the silver layer to prevent corrosion or atomic migration in that region. On the CrN_x adhesion layer mirror, as reactant enters the coating layers through a central defect in the SiN_x overcoat, the corrosion reaction is supplied by material from the top of the Ag layer. In the mirror with the $NiCrN_x$ adhesion layer, better adhesion at the Ag-SiN_x interface turns off the reactant supply at that interface. The more favored nickel corrosion reaction is then supplied by material from the bottom of the silver layer at the NiCr-Ag interface.

The sacrificial nickel corrosion reaction provides insight into the large size of the circular diffusion regions on the mirror with the CrN_x adhesion layer compared to the smaller ones on the mirror with the $NiCrN_x$ adhesion layer. In the CrN_x adhesion layer mirror, atomic migration proceeds readily at the Ag-SiN_x interface, forming the large diffusion regions; the corrosion reaction does not extend to material from the lower NiCr-Ag interface. In the $NiCrN_x$ adhesion layer mirror, the reactant supply from the top of the Ag layer is limited due to improved adhesion at the Ag-SiN_x interface. The ensuing supply of material from the NiCr-Ag interface results in the smaller size of the diffusion regions on the $NiCrN_x$ adhesion layer mirror.

In the previous section, it was suggested that better adhesion at the NiCr-Ag interface could slow atomic migration there to further improve corrosion resistance. The reduced adhesion

resulting from the CrN_x adhesion layer compared to the $NiCrN_x$ adhesion layer, suggests that $NiCrN_x$ beneath the Ag layer could improve adhesion at the NiCr-Ag interface. This could take the form of a thin $NiCrN_x$ interlayer between the NiCr and Ag layers, or a thick layer of $NiCrN_x$ beneath the Ag in place of the existing NiCr layer, as previous researchers have recommended [12]. The $NiCrN_x$ could serve to pin the layers together to reduce the corrosion and atomic migration along the NiCr-Ag interface. This would likely affect the sacrificial corrosion reaction of the nickel from the NiCr base layer; the effect of this change on the silver is not immediately clear. Because the corrosion of nickel in the $NiCrN_x$ adhesion layer mirror appears to dominate the corrosion process, the silver corrosion reaction is clearly not favored. Thus, a $NiCrN_x$ adhesion layer beneath the Ag layer could force the silver corrosion reaction to occur, potentially changing the dynamics of the entire corrosion process. This behavior is currently being investigated.

Ultimately, the composition of the thin adhesion layer dramatically changes the nature of the Ag-SiN_x interface. Compared to CrN_x, the thin layer of $NiCrN_x$ significantly improves adhesion at that interface, slowing corrosion and atomic migration there. However, considerable corrosion and atomic migration results at the NiCr-Ag interface in the $NiCrN_x$ adhesion layer mirror; this leads to silver agglomeration and a corresponding increase in scatter. These significant differences in the corrosion behavior illustrate the large difference that the small amount of nickel makes. Even so, neither mirror experienced substantial degradation nor a loss in reflectance after 242 hr of MFG exposure, indicating that both $NiCrN_x$ and CrN_x make good adhesion layer materials and improve the corrosion resistance of plasma beam sputtered silver mirrors. The differences in the corrosion behavior serve to illuminate the mechanism by which $NiCrN_x$ improves durability, suggesting ways to make even more durable mirrors.

6. Conclusion

Accelerated environmental exposure testing and multiple analytical techniques were used to investigate the corrosion behavior of protected silver mirrors prepared by plasma beam sputtering. Various mirrors with different adhesion and protection layers were compared with respect to optical performance and durability. The corrosion features on these mirrors were evaluated to better understand the mechanism by which the adhesion and protection layers improve mirror durability.

Salt fog exposure of plasma beam sputtered silver mirrors correlated with similar testing of magnetron sputtered silver mirrors. As expected, mirrors without both an adhesion and a protection layer experienced significant corrosion, which markedly reduced reflectance and increased scatter. Mirrors with both the adhesion and protection layers showed dramatically improved corrosion resistance. The plasma beam sputtered mirrors in this study exhibited similar degradation behavior to the previous mirrors and are likely influenced by similar corrosion phenomena.

Mixed flowing gas exposure of plasma beam sputtered silver mirrors showed more subtle differences in corrosion behavior between the mirrors with different adhesion layer materials. None of the mirrors experienced significant loss in reflectance, and only small increases in scatter were observed. However, degradation was apparent, with significant differences in corrosion feature morphology due to the composition of the adhesion layer. In the mirror with the CrN_x adhesion layer, large circular diffusion regions formed due to silver migration from the top of the silver layer, at the Ag-CrN_x-SiN_x interface. Comparatively, the mirror with the $NiCrN_x$ adhesion layer showed much smaller diffusion regions that were driven by silver migration from the bottom

of the silver layer, at the NiCr-Ag interface. Interestingly, the SiN_x overcoats were largely intact across the corrosion features on both mirrors. The small amount of nickel in the adhesion layer clearly has a significant impact on the Ag-SiN_x interface, which, in turn, affects the corrosion behavior. XPS data indicated nickel penetrated further into the silver layer than CrN_x, suggesting that the nickel-silver interaction promotes better adhesion of the dielectric to the silver, preventing atomic migration at that interface.

The lateral migration of silver, and not just corrosion of silver, was found to be a more important aspect of the corrosion process than initially believed. In the $NiCrN_x$ adhesion layer mirror, lateral migration of silver resulted in significant silver voiding as well as substantial silver agglomeration. This silver agglomeration increased the measured scatter and surface roughness, correlating the morphology of the corrosion features to the resulting optical properties. Moreover, the silver migration did not appear to be driven by an electrochemical potential. Rather, it was more likely the result of sacrificial nickel corrosion reactions. With atomic migration at the Ag-SiN_x interface limited by the $NiCrN_x$ adhesion layer, the nickel in the NiCr base layer encountered a larger driving force to react. Together, the silver and nickel migration indicate that the lower NiCr-Ag interface, and not just the upper Ag-SiN_x interface, plays an important role in the corrosion process. Better adhesion at the lower interface is necessary to improve mirror durability.

While the $NiCrN_x$ adhesion layer is important in nucleating a dense SiN_x protection layer, that is only a part of the mechanism of protection. Better adhesion at all layer interfaces is clearly important in improving mirror durability as well. Future work will continue to focus on these protection mechanisms. Analysis of the CrN_x adhesion layer mirror will be continued. Other adhesion layer materials, such as NiCr and Cr, will also be studied to better understand how the nitride materials interact to improve corrosion resistance. Furthermore, multiple dielectric

enhancement layers will be investigated regarding the additional protection they afford while also improving optical performance. Finally, the effects of the accelerated testing environment, such as the incremental stopping of the exposures for analyses, will be examined to better correlate with real long-term environmental exposure behavior.

This thesis illuminates the mechanisms by which nichrome nitride and other adhesion layer materials improve silver mirror durability. However, there is still much to be determined. The search continues for better adhesion and protection layer materials that provide improved corrosion resistance without degrading silver's high reflectivity. Control of the environment, by reducing the level of moisture as well as the levels of known contaminants, continues to be critical for long term durability. Moreover, the composition of the adhesion layer, the level of adhesion at the layer interfaces, and the ability to limit silver migration are all important factors in corrosion resistance. Silver continues to be the material of choice for the most demanding optical applications, requiring the development of ever more durable mirrors.

References

[1] M. Boccas, T. Vucina, C. Araya, E. Vera and C. Ahhee, "Protected-silver coatings for the 8-m Gemini telescope mirrors," *Thin Solid Films,* vol. 502, pp. 275-280, 2006.

[2] H. Ford, P. Feldman, D. Golimowski, Z. Tsvetanov, F. Bartko, J. Crocker, P. Bely, R. Brown, C. Burrows, M. Clampin, G. Hartig, M. Postman, M. Rafal, W. Sparks, R. White, T. Broadhurst, G. Illingworth, T. Kelly, B. Woodruff, E. Cheng, R. Kimble, C. Krebs, S. Neff, M. Lesser and G. Miley, "The advanced camera for the Hubble Space Telescope," in *Proc. SPIE vol. 2807*, pp. 184-186, 1996.

[3] N. Thomas and J. Wolfe, "UV-shifted durable silver coating for astronomical mirrors," in *Proc. SPIE vol. 4003*, Optical Design, Materials, Fabrication, and Maintenance, pp. 312-323, 2000.

[4] D.-Y. Song, R. W. Sprague, H. A. Macleod and M. R. Jacobson, "Progess in the development of a durable silver-based high-reflectance coating for astronomical telescopes," *Appl. Opt.,* vol. 24, no. 8, pp. 1164-1170, 1985.

[5] D. A. Sheikh, S. J. Connell and R. S. Dummer, "Durable silver coating for Kepler Space Telescope primary mirror," in *Proc. SPIE vol. 7010*, Space Telescopes and Instrumentation, 70104E, 2008.

[6] J. L. Daniel and J. E. Coleman, "Progressive changes in microstructure and composition during degradation of solar mirrors," *Sol. Energy Mater.,* vol. 3, pp. 135-150, 1980.

[7] H. E. Bennett, R. L. Peck, D. K. Burge and J. M. Bennett, "Formation and growth of tarnish on evaporated silver films," *J. Appl. Phys.,* vol. 40, no. 8, pp. 3351-3360, 1969.

[8] T. E. Graedel, "Corrosion mechanisms of silver exposed to the atmosphere," *J. Electrochem. Soc.,* vol. 139, no. 7, pp. 1963-1970, 1992.

[9] J. D. Barrie, P. D. Fuqua, K. A. Folgner and C.-T. Chu, "Control of stress in protected silver mirrors prepared by plasma beam sputtering," *Appl. Opt.,* vol. 50, no. 9, pp. C135-C140, 2011.

[10] S. F. Pellicori, "Scattering defects in silver mirror coatings," *Appl. Opt.,* vol. 19, no. 18, pp. 3096-3098, 1980.

[11] C. T. Chu, P. D. Fuqua and J. D. Barrie, "Corrosion characterization of durable silver coatings by electrochemical impedance spectroscopy and accelerated environmental testing," *Appl. Opt.,* vol. 45, no. 7, pp. 1583-1593, March 2006.

[12] J. D. Wolfe, R. E. Laird, C. K. Carniglia and J. P. Lehan, "Durable silver-based antireflection coatings and enhanced mirrors," in *Optical Interference Coatings*, vol. 17, Technical Digest Series, Optical Society of America, pp. 115-117, 1995.

[13] G. Hass, "Reflectance and preparation of front-surface mirrors for use at various angles of incidence from the ultraviolet to the far infrared," *J. Opt. Soc. Am.,* vol. 72, no. 1, pp. 27-39, 1982.

[14] D. K. Burge, H. E. Bennett and E. J. Ashley, "Effect of atmospheric exposure on the infrared reflectance of silvered mirrors with and without protective coatings," *Appl. Opt.,* vol. 12, no. 1, pp. 42-47, 1973.

[15] D. W. Rice, P. Peterson, E. B. Rigby, P. B. P. Phipps, R. J. Cappell and R. Tremoureux, "Atmospheric corrosion of copper and silver," *J. Electrochem. Soc.,* vol. 128, no. 2, pp. 275-284, 1981.

[16] D. A. Sheikh, "Improved silver mirror coating for ground and space-based astronomy," in *Proc. SPIE vol. 9912*, Advances in Optical and Mechanical Technologies for Telescopes and Instrumentation II, 991239, 2016.

[17] Y. Ben Amor, E. M. Sutter, H. Takenouti, M. E. Orazem and B. Tribollet, "Interpretation of electrochemical impedance for corrosion of a coated silver film in terms of a pore-in-pore model," *J. Electrochem. Soc.,* vol. 161, no. 14, pp. C573-C579, 2014.

[18] P. D. Fuqua and J. D. Barrie, "Optical properties and corrosion resistance of durable silver coatings," in *Mat. Res. Soc. Symp. Proc. vol. 555*, pp. 85-90, 1999.

[19] C.-T. Chu, P. D. Chaffee, C. J. Panetta and J. D. Barrie, "Mixed flowing gas testing of silver mirror coatings," in *Optical Interference Coatings*, OSA Technical Digest (Optical Society of America), paper TuEPDP5, 2007.

[20] A. C. Phillips, D. M. Fryhauf and N. P. Kobayashi, "Progress and new techniques for protected-silver coatings," in *Proc. SPIE vol. 9151*, Advances in Optical and Mechanical Technologies for Telescopes and Instrumentation, 91511B, 2014.

[21] D. M. Fryhauf, A. C. Phillips and N. P. Kobayashi, "Corrosion barriers for silver-based telescope mirrors: comparative study of plasma-enhanced atomic layer deposition and reactive evaporation of aluminum oxide," *J. Astron. Inst. Sys.,* vol. 1, no. 4, 2015.

[22] S. Schwinde, M. Schurmann, P. J. Jobst, N. Kaiser and A. Tunnermann, "Description of particle induced damage on protected silver coatings," *Appl. Opt.,* vol. 54, no. 16, pp. 4966-4971, 2015.

[23] P. J. Kelly and R. D. Arnell, "Magnetron sputtering: a review of recent developments and applications," *Vacuum,* vol. 56, no. 3, pp. 159-170, 2000.

[24] D. L. Smith, Thin Film Deposition: Principles & Practice, Boston: McGraw-Hill, Inc., 1995.

[25] M. J. Thwaites, "High density plasmas," U.S. Patent 6,463,873, 15 October 2002.

[26] *ASTM B117-16 Standard Practice for Operating Salt Spray (Fog) Apparatus,* West Conshohocken, PA: ASTM International, 2016.

[27] *ASTM B827-05 Standard Practice for Conducting Mixed Flowing Gas (MFG) Environmental Tests,* West Conshohocken, PA: ASTM International, 2014.

[28] C.-T. Chu, D. R. Alaan and D. P. Taylor, "Accelerated atmospheric corrosion testing of electroplated gold mirror coatings," in *Proc. SPIE vol. 7786*, Current Developments in Lens Design and Optical Engineering XI and Advances in Thin Film Coatings VI, 77860J, 2010.

[29] C.-T. Chu, C. J. Panetta and D. R. Alaan, "Mixed-flowing-gas testing of gold mirror coatings," in *Optical Interference Coatings*, OSA Technical Digest (Optical Society of America), 2010.

[30] W. H. Abbott, "The development and performance characteristics of mixed flowing gas test environment," *IEEE Trans. Compon., Hybrids, Manuf. Technol.,* vol. 11, no. 1, pp. 22-35, 1988.

[31] L. A. Giannuzzi and F. A. Stevie, "A review of focused ion beam milling techniques for TEM specimen preparation," *Micron,* vol. 30, no. 3, pp. 197-204, 1999.

[32] I. Petrov, P. B. Barna, L. Hultman and J. E. Greene, "Microstructural evolution during film growth," *J. Vac. Sci. Technol. A,* vol. 21, no. 5, pp. S117-S128, 2003.

[33] J. A. Thornton, "The microstructure of sputter-deposited coatings," *J. Vac. Sci. Technol. A,* vol. 4, no. 6, pp. 3059-3065, 1986.